# Mature riparian alder forest acts as a strong and consistent carbon sink

Alisa Krasnova<sup>1,2</sup>, Kaido Soosaar<sup>1</sup>, Svyatoslav Rogozin<sup>1</sup>, Dmitrii Krasnov<sup>3</sup>, Ülo Mander<sup>1</sup>

<sup>1</sup>Department of Geography, Institute of Ecology and Earth Sciences, University of Tartu, Tartu, 50090, Estonia <sup>2</sup>Department of Forest Ecology and Management, Swedish University of Agricultural Sciences, Umeå, 90183, Sweden <sup>3</sup>Institute of Forestry and Engineering, Estonian Life Science University, Tartu, 51006, Estonia \*\*Correspondence to: Alisa Krasnova (alisa.krasnova@ut.ee)

Abstract. Alder forests are widely spreadwidespread across the Northern Hemisphere, frequently often occupying riparian buffer zones and playing a key role in enhancing soil fertility through symbiosis with nitrogen-fixing bacteria. Despite their ecological significance, studies on importance, the ecosystem-level carbon (C) and water (H2O) exchange inof alder forests remain searce remains poorly studied, particularly in the context of under contrasting hydroclimatic variability and extreme weather events conditions. In this study, we used eddy-covariance flux measurements from measured ecosystem carbon and water fluxes over three contrasting years to assess the C balance and H<sub>2</sub>O exchange of ("wet", "drought", "recovery") in a mature riparian grey alder forest in the hemiboreal zone in Estonia. The siteforest was a strong and consistent net carbon sink with annual net ecosystem exchange (NEE) ranging from -496 to -663 g C m<sup>-2-2</sup> y<sup>-1-1</sup> gross primary production (GPP) from -1258 to -1420 g C m<sup>-2-2</sup> y<sup>-1</sup> and evapotranspiration (ET) from 595 to 923 g C m<sup>-2-2</sup> y<sup>-1</sup> and evapotranspiration (ET) varied from 194 to 342 kg H<sub>2</sub>O m<sup>-2-2</sup> y<sup>-1</sup> and ecosystem water use efficiency (EWUE) was 4.2 - 6.5 g C kg H<sub>2</sub>O<sup>-1</sup>. The drought and heatwave year (2018) featured the highest net carbon uptake, driven by an increase in GPP during spring and a reduction in ER during late summer and autumn. A minor impact of 1. Moderate soil water saturation (40-50%) enhanced all ecosystem fluxes. In contrast, progressive drought on GPP combined reduced ER, ET, and to a lesser extent GPP, with a 35% reduction in ET in 2018 lead to peak values of EWUE in response to H2O limitation. In 2019, we found no evidence of a short-term drought legacy effect, as carbon exchange components recovered to the 2017 levels and ET was the highest out of years. Given that this forest is beyond the typical harvestable age, its-elevated EWUE and suppressed canopy conductance indicating strong and consistentstomatal regulation to limit water loss while maintaining efficient carbon sequestration, combined with high short term. While soil saturation affected canopy conductance, its effect was outweighed by vapour pressure deficit during the drought year, even after soil water availability recovered. We observed a full recovery in the following year, which was supported by favourable temperature and precipitation, although partially suppressed canopy conductance suggested some vulnerability to possible consecutive droughts in the future. Overall, the forest demonstrated drought resilience, provides valuable insights for sustainable forest management. These findings highlight the potential and high net carbon uptake across contrasting years, underscoring the capacity of riparian grey-alder forestsstands to maintain productivitysustain carbon sequestration under variable hydroclimatic variability, reinforcing their role in regional earbon cycling as a part of natural climate mitigation solutions conditions.

#### 1. Introduction

20

35 Terrestrial ecosystems play an essential role in mitigatingslowing the rise of atmospheric carbon dioxide (CO<sub>2</sub>) concentrations and restraining global warming (Pan et al., 2011; Piao et al., 2020). Over the preceding decades, they have effectively sequestered approximately one-third of the total industrial carbon —(C) emissions (Friedlingstein et al., 2022). Forest ecosystems, in particular, typically act as net C sinks, with the rate of photosynthetic uptake surpassing respiratory emissions on the annual scale (Harris et al., 2021). However, The strength of this Ccarbon sink is contingent depends upon various factors,

40 including, but not limited to, forest age, tree species composition, climatic conditions, soil properties, and management practices (Winkler et al., 2023). Moreover, under certaina change in weather conditions, or forest management decisions can turn a local Ccarbon-sequestering forest may transition to a state of C neutrality or even becomestand into a net Ccarbon source, thereby affecting ecosystem-atmosphere interactions at a regional scale (Hadden and Grelle, 2016; Lindroth et al., 1998). ThereforeThus, it is critical to evaluate the sustainability of a local forest elimate mitigation potential carbon uptake in the face of varying climatic events (Allen et al., 2010; Bonan, 2008; Teskey et al., 2015).

Water availability is one ofplays a particularly critical role among the crucial environmental factors inaffecting forest survival, and droughts could be one of the key reasons for forestcarbon uptake. Drought can reduce photosynthesis, increase tree mortality, and temporarily weaken or reverse a forest's sink function (Allen et al., 2010; Breshears et al., 2005; Cavin et al., 2013; Haberstroh et al., 2022; McDowell et al., 2008). The frequency and severity of extreme climate events, including droughts, have been growing in recent decades—and are, a trend expected to continue in the future (Fischer et al., 2021; Trenberth et al., 2014). In The 2018, Europe faced a European drought that was considered the most severe in the last 250 years (Gutierrez Lopez et al., 2021; Hari et al., 2020), eausing reduced Cresulting in a significant decline in forest carbon uptake and elevated tree mortality rates (Bastos et al., 2020; Buras et al., 2020; Haberstroh et al., 2022; Senf and Seidl, 2021; Smith et al., 2020). Thus, it is essential to quantify the C uptake capacities Improving our understanding of different forests bothhow forest carbon and water fluxes are modified during and following drought conditions to better understand theirafter such events is crucial for assessing ecosystem resilience and informinforming adaptive forest management—strategies for enhancing forest sustainability.

Riparian forests, located at the interface between terrestrial and aquatic systems, play a crucial role in mediating nutrient and carbon flows and are particularly sensitive to hydrological changes (Capon et al., 2013; Dybala et al., 2019; Naiman and Décamps, 1997). Grey alder (Alnus incana (L.) Moench.) is a typical pioneer species frequently occupying riparian zones and is widely spread in North America and Europe (Caudullo et al., 2017). Alder plantations can mitigate Ccarbon losses in rewetted peatlands (Huth et al., 2018) and improve the soil structure of skid trails (Warlo et al., 2019). Their high adaptability also makes alders suitable for the afforestation of post-industrial sites (Krzaklewski et al., 2012). Owing to their symbiosis with atmospheric nitrogen-fixing bacteria (Benson, 1982; Rytter et al., 1989), alder trees play an essential role in forest soil nitrogen enrichment (Mander et al., 2008, 2021; Soosaar et al., 2011). Moreover, Due to their rapid growth, alder species are frequently chosen for riparian buffer zones and short-rotation forestry (Aosaar et al., 2012; Rytter and Rytter, 2016; Uri et al., 2017). However, there are surprisingly few studies on the C uptake potential and water use efficiency of alder forests, particularly in the context of extreme weather events.

The net ecosystem production (NEP) of a grey alder forest chronosequence in Estonia was previously estimated by Uri at al.

(2017), utilising the traditional C budgeting method. Their findings indicated that while most grey alder stands functioned as C sinks, a young (9 year old) and a mature (40 year old) site acted as moderate C sources. This was attributed to elevated heterotrophic respiration at both sites and, in the case of the young stand, low net primary production. However, the authors noted that interannual variations in NEP were primarily driven by climatic factors rather than stand age. These findings highlight the need for further assessments of net C uptake under varying weather conditions, particularly in mature grey alder

However, ecosystem-level studies on carbon and water exchange in alder forests remain extremely limited. At the time of manuscript preparation, only two studies had reported ecosystem carbon exchange in grey alder forests. Uri et al. (2017) estimated net ecosystem production across an alder chronosequence using the carbon budgeting method. While informative, this traditional approach relies on discrete estimates of multiple carbon pools and fluxes and typically provides only an annual-scale assessment. In contrast, the eddy-covariance (EC) method provides continuous, high-frequency measurements of carbon and water fluxes between the ecosystem and the atmosphere, allowing for the detection of intra-annual dynamics that can strongly influence the annual balance (Baldocchi, 2014). In our previous study (Krasnova et al., 2022), we conducted a two-

year comparative analysis of EC carbon fluxes across four different forested ecosystems, including the current site. That study focused on the effects of elevated air temperatures on carbon exchange and found that spring warming enhanced carbon uptake in the alder forest, indicating a positive temperature response during the early growing season. However, the analysis did not address soil moisture variability, water fluxes, or post-drought recovery dynamics, leaving a substantial gap in our understanding of alder forest functioning.

In this study, we aim to investigate the Cecosystem-level carbon and water exchange of a mature riparian alder forest stand in the hemiboreal zone. While our previous research (Krasnova et al., 2022) examined how several forested ecosystems in Estonia responded to elevated temperatures during the in Estonia in relation to soil moisture variability. We utilise three years of EC flux measurements, representing a "wet" year (2017), a "drought" year (2018 heatwave, water fluxes were not analysed. Moreover, the effects of stress factors on forest ecosystems can become more pronounced in the years following exposure (Anderegg et al., 2015; Kannenberg et al., 2020), which was beyond the scope of our previous study. Therefore, the ), and a "recovery" year (2019). The specific objectives of this study are to (1):

(1) quantify the Cannual carbon and water exchange of in an alder forest under varying hydroclimatic conditions; (2) investigate over three contrasting years;

(1)(2) <u>assess</u> the influence of <u>differentyarying</u> soil moisture <u>regimes on alder forest C exchange conditions;</u> and

2)(3) \_\_\_\_\_water use efficiency; (3) evaluate the presence of legacydrought recovery and carry-over effects and the long term sustainability of grey alder forests as a nature-based solution for climate mitigation.

## 2. Methods

85

90

95

100

#### 2.1 Study site and footprint area

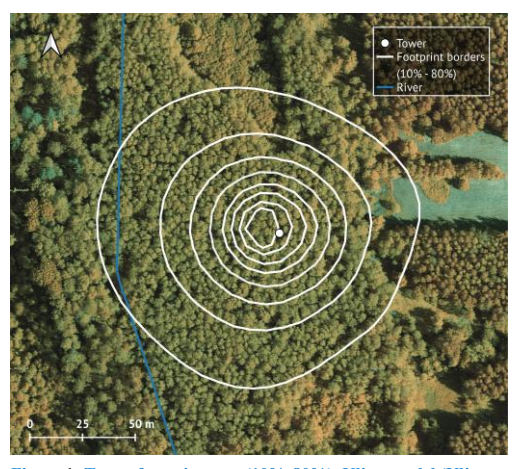


Figure 1: Tower footprint area (10%-80%), Kljun model (Kljun et al., 2015); the blue line indicates the location of Kalli River, Mapdata: Estonian Land Board (Maa-amet), accessed via QGIS in 2023.

The ecosystem in our study is a mature 40-year-old riparian grey alder (Alnus incana (L.) Moench) forest stand located on a former agricultural landthat established naturally following the abandonment of a wet meadow formerly used for haymaking and livestock grazing in southern Estonia. The terrain is flat, formed at the bottom of former periglacial lake systems, with an average elevation of 32 m a.s.l. and a 1% inclination slope towards a tributary of the Kalli River. The average annual air temperature is 5.8 °C, whereas in July and January, the mean air temperatures are 17.0 °C and 6.7 °C, respectively (Kupper et al., 2011). The soil is Glevic Luvisol, with a 15-20cm humus layer. The top 10 em soil C and N content were 3.8% and 0.33% (Mander et al., 2022), resulting in the C:N ratio of 11.5.over the ten years before the study (2006 - 2016) was 6.6 °C with 627 mm year-1 of precipitation (Eesti Keskkonnaagentuur). The soil at the study site is classified as a Gleyic Luvisol, a

hydromorphic soil type typical of seasonally waterlogged riparian zones. The humus layer thickness is 15-20 cm. The upper soil layer is moderately fertile, with a relatively high organic matter content, moderate total carbon and nitrogen concentrations, and a balanced C:N ratio (Table C1). Bulk density is relatively high, suggesting some compaction, likely due to past land use

and seasonal wetting and drying cycles. Poor drainage and a fine-textured subsoil limit infiltration, making the site sensitive to both waterlogging and rapid topsoil drying during drought.

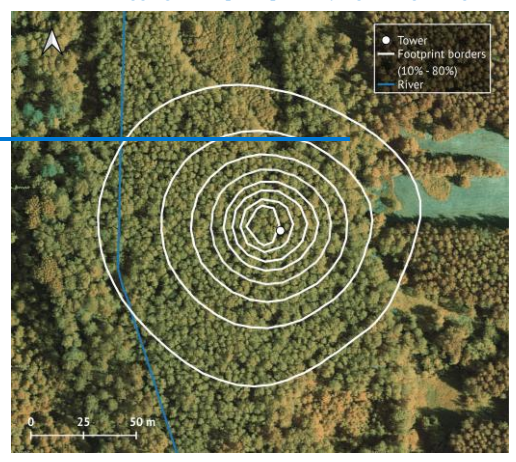


Figure 1: Tower footprint area (10%-80%), Kljun model (Kljun et al., 2015); the blue line indicates the location Kalli River. Map data: Estonian Land Board (Maa-amet), accessed via QGIS.

The total footprint area (Fig. 1) is 1.65 ha, 85% of which (1.41 ha), is covered by grey alder. The footprint area of the tower (Figure 1) is 1.65 ha, 85% of which (1.41 ha) is covered by grey alder. The river, birch and spruce trees and a narrow section of the adjacent clear-cut represent the remaining area at the edges of the footprint. The average stand height is 17.5 m, the stand density is 1520 trees per ha, the mean stem diameter at breast height is 15.6 cm, and the basal area is 30.5 m² ha⁻¹ (Mander et al., 2022). The understory is dominated by herbs (Filipendula ulmaria (L.) Maxim., Aegopodium podagraria L., Cirsium oleraceum (L.) Scop., Geum rivale L., Crepis paludosa L., mosses (Climacium dendroides (Hedw.) F. Weber & D. Mohr, Plagiomnium spp. and Rhytidiadelphus triquetrus (Hedw.) Warnst. Moench; shrubs (Rubus idaeus L., Frangula alnus L., Daphne mezereum L.) and young trees (Alnus incana, Prunus padus L.).

## 2.2 Instrumentation

125

130

145

The eddy-covariance (EC) setup consisted of a fast 3-D sonic anemometer Gill HS-50 (Gill Instruments Ltd., Lymington, Hampshire, UK) and enclosed CO<sub>2</sub> and H<sub>2</sub>O gas-analyser LI-7200 (LI-COR Biosciences, Lincoln, NE, USA) measuring with 10Hz frequency. The instruments were mounted on top of a 21m scaffolding tower in spring 2017; with the first measurements started starting on the 15<sup>th</sup> of May 2017. Air temperature and humidity (Rotronic HC2A-S3; Rotronic AG, Bassersdorf, Switzerland) and photosynthetically active radiation (PAR; LI-190SL; LI-COR Biosciences, Lincoln, NE, USA) were measured in a tower at 5 m height for air temperature and relative humidity and 25 m height for PAR (above the forest canopy).

Twelve soil temperature (107, CAMPBELL SCIENTIFIC—Ine., INC, Logan, Utah, USA) and soil water content (ML3 ThetaProbe, Delta-T Devices, Burwell, Cambridge, UK) sensors were installed at 10 cm depth in the end of July 2017. WTD was measured manually in groundwater wells next to the soil chambers on each sampling day Precipitation data were obtained from a nearby station, located around 2 km away from the site.

## 2.3 Fluxes calculation and post-processing

The fluxes of CO<sub>2</sub> and latent heat (LE) were calculated as a covariance between vertical wind speeds and CO<sub>2</sub> (or H<sub>2</sub>O) concentrations using EddyPro software (version 6.3.0, LI-COR Biosciences, USA) and averaged over the 30-minute intervals. In the absence of a storage measuring profile system, we estimated flux storage using the tower-top method, which utilised half-hourly CO<sub>2</sub> concentration measurements from the EC system. Net ecosystem exchange (NEE) was then calculated as the

sum of eddy flux and storage. To eliminate periods of underdeveloped turbulence, we applied friction velocity filtering; the thresholdthresholds of 0.28 m s<sup>-1</sup> for 2017-2018 and 0.22 m s<sup>-1</sup> for 2019 were calculated with a moving point test (Papale et al., 2006). Fluxes during the half-hours with friction velocity values below these thresholds were removed from the analysis. To ensure adequate mixing conditions throughout the measurement period, we opted to remove not only nighttime half-hours, but also daytime NEE values associated with low friction velocity estimates.

In a previous study conducted at the same site by Mander et al. (2022) considered unaccounted), we noted that strong advection

160

as a possible reason formight be a feature of this forest site, with a rather dense canopy during the discrepancy between soilactive vegetation period and ecosystem scale fluxesa slight inclination towards the river tributary. To identify the periods when advection was significant, we applied the filtering method following Wharton et al. (2009) and Chi et al. (2019). Turbulence intensity parameters (I<sub>w</sub> and I<sub>u</sub>) were calculated for each half-hour as the ratios of vertical and horizontal wind velocity to turbulence intensity, respectively. For any half-hour, if I<sub>w</sub> or I<sub>u</sub> was outside of the window of mean plus one standard deviation estimated for the entire measurement period, advective conditions during this half-hour were considered non-negligible, and NEE and LE were filtered out. The remaining spikes in the dataset could be attributed to the simplification of the flux storage calculation procedure or the instrumental failure. Therefore, fluxes outside the common range (mean ± 3 × × standard deviation) were filtered out over a 14-day moving window (151 half-hour values). Overall, After all the final quality-controlled values were filtering steps, 60% in 2017, 66% in 2018 and 65% in 2019. Evapotranspiration (ET) was then calculated by dividing the filtered LE by the latent heat of vaporisation (Allen et al., 1998). Quality-controlled values remained. Evapotranspiration (ET) was calculated by dividing the filtered LE by the latent heat of vaporisation (Allen et al., 1998). Energy balance closure (EBC) was 70%, 71% and 80% in 2017, 2018 and 2019, respectively (Figure A1). Given the simplified estimation of available energy in the absence of direct net radiation and ground heat flux measurements (see Appendix A for details), we chose not to apply any EBC correction to LE. This avoids introducing additional uncertainty and ensures that year-

In order to obtain fluxes aggregated over various time scales, we gap-filled NEE and ET using XGBoost as recommended by Vekuri et al. (2023). The hyperparameters were tuned during 5-fold cross-validation and included maximum tree depths (3, 5, 10, 15), regularization strength with default 0, data sampling ratios (0.5, 0.75, 1), feature sampling ratios (0.4, 0.6, 0.8, 1), and minimum child weights (2, 5, 10). The hyperparameters were determined using all available data. A squared loss with a default learning rate of 0.1 was used as an objective function.

The partitioning of NEE into gross primary production (GPP) and ecosystem respiration (ER) was performed with the "nighttime" method <u>utilisingin</u> the ReddyProcWeb tool (Wutzler et al., 2018). Nighttime respiration was considered equal to nighttime gap-filled NEE values, while daytime ER was modelled in ReddyProcWeb using the air temperature dependence of measured nighttime values (Eq. 1)

$$ER = ER_{re}e^{E_0\left(\frac{1}{T_{ref}-T_0} - \frac{1}{T-T_0}\right)}$$
 (1)

where  $R_{ref}$  (µmol m<sup>-2</sup> s<sup>-1</sup>) is the respiration at the reference temperature; E0 (kJ mol<sup>-1</sup>) is the activation energy; T (°C) is the measured air temperature.  $T_{ref}$  was set to 15 °C, and  $T_0$  was kept constant at -46.02 °C following Lloyd and Taylor (1994). -GPP was then calculated as athe difference between gap-filled NEE and modelled ER. We chose to use the nighttime flux partitioning method because, unlike the daytime ERmethod, where GPP is modelled, here GPP is derived indirectly as a residual. This approach allowed us to further calculate canopy physiological response parameters. Following the micrometeorological convention, negative flux denotes uptake, while positive flux is a release from the ecosystem into the atmosphere.

#### 2.4 Additional Canopy physiological response parameters and statistical analysis

to-year comparisons of ET remain internally consistent.

To quantify forest resistance and resiliencestudy the physiological response of the ecosystem to varying soil moisture conditions, we estimated two calculated additional parameters: ecosystem water use efficiency (EWUE) as), canopy

photosynthetic capacity (GPP<sub>sat</sub>) and canopy conductance (Gc). Since these parameters characterise the vegetation activity, 195 they were computed only for dry- (rainfall less than 1 mm d<sup>-1</sup>) active-canopy (GPP <-1 g C m<sup>-2</sup> d<sup>-1</sup> and ET > 0.25 mm d<sup>-1</sup>) days during the growing seasons. The start and end of each growing season were estimated by fitting a double-logistic curve to daily GPP sums and identifying the inflexion points, as outlined in Gonsamo et al. (2013). Canopy EWUE and Gc were calculated using only half-hours with sufficient light conditions. The threshold global radiation (Rg) value of 435 W m<sup>-2</sup> was computed from the bin-averaged GPP-Rg response curve in summer (JJA) dry- and active-canopy days of all three years using breakpoint analysis to identify the flattening point of the curve. 200

Ecosystem water use efficiency (EWUE), defined as the amount of carbon obtained by the forest per unit of water lost to the atmosphere, can serve as an indicator of a forest's adaptability to changes inchanging water resources availability (Huang et al., 2015; Keenan et al., 2013; Yang et al., 2016), and canopy photosynthetic capacity (GPPsat) as a measure of the ecosystem's functional stability (). We calculated EWUE as the ratio of the sum of absolute GPP values to the sum of ET, using two approaches. First, to compute annual and May-September EWUE, we used period sums of GPP and ET, including all data points. Second, to characterise canopy-specific EWUE, we calculated daily values focusing solely on periods of active photosynthesis and transpiration. For this, we included only half-hourly measurements taken under sufficient light conditions and restricted calculations to dry, active-canopy days within the growing seasons. Although we did not explicitly partition ET into evaporation and transpiration components, our filtering approach ensures that canopy-driven water fluxes dominate the 210 ET.

205

220

225

Canopy photosynthetic capacity (GPPsat) represents the forest's carbon uptake potential, i.e. how much carbon the ecosystem can sequester when light is not limiting (Aubinet et al., 2012; Chen et al., 2023; Fleischer et al., 2013; Musavi et al., 2017). EWUE was calculated as a ratio of GPP to ET.

; Xu et al., 2020a). To obtain GPP<sub>sat</sub>, we used a modified version of the rectangular hyperbolic light response curve (Eq. 1), 215 that was Michaelis-Menten photosynthetic response model (Michaelis and Menten, 1913), fitted to half-hourly daytime (Rg > 15 W m<sup>-2</sup>) GPP and global radiation data (Eq. 2). The fits were done in 3-day running windows, using a 5-day moving only dry and active-canopy days, and parameters we assigned to the middle of each window.

$$GPP = \frac{\alpha GPP_{max} R_g}{\alpha R_s + GPP_{max}}$$
 (2)

Where  $\alpha$  (µmol J<sup>-1</sup>) is the canopy light utilisation efficiency; GPP<sub>max</sub> (µmol m<sup>-2</sup> s<sup>-1</sup>) is the maximum GPP; Rg is global radiation  $(W m^{-2})$ 

We chose this simplified the rectangular form of the light response curve-equation over the more detailed non-rectangular version used by one (Chen et al., 2023; Gilmanov et al., 2003; Musavi et al., 2017) and Chen et al. (2023) because it demonstrated considerably better performance (a higher number of successful fits) with our dataset. However, a limitation of the simpler model is that the estimated GPP<sub>max</sub> does not always correspond to the actual light saturation point. Therefore, we computed GPP<sub>sat</sub> as GPP at Rg of 1000 W m<sup>-2</sup>. Only the values from windows with significant fit parameters (p<0.05) and R<sup>2</sup>>0.5 were retained. For clarity in describing GPP<sub>sat</sub> variability, we use its absolute values, omitting the negative sign that typically denotes flux direction.

Canopy conductance (GcGPP = 
$$\frac{\text{cGPP}_{mem} \cdot P_{e}}{\alpha R_{g} + \text{GPP}_{mem}}$$

230 where α (μmol J<sup>-1</sup>) is thea representation of stomatal conductance on the ecosystem level. We computed Gc by the inversion of the Penman-Monteith equation (Eq. 3,4) only for the dry active canopy under sufficient light utilisation efficiency; (Rg ≥ 435 W m<sup>-2</sup>):

$$G_c^{-1} = \frac{\rho_a c_p \left(\frac{\text{VPD}}{LE}\right)}{\gamma} + \left(\frac{\Delta}{\gamma} \beta - 1\right) g_a^{-1} \tag{3}$$

235  $g_a^{-1} = \frac{\mu}{u^2} + 6.2\mu_*^{-2/3}$  (4)

Where  $\rho_a$  is global radiation; GPP<sub>max</sub> (µmolthe air density (kg m<sup>2</sup>-s<sup>-1</sup>)<sup>3</sup>);  $C_p$  is the maximum GPP,  $ER_{day}$  (µmol m<sup>-2</sup>specific heat capacity of air (J kg K<sup>-1</sup>); VPD is vapour pressure deficit (kPa); LE is latent heat flux (W m<sup>-2</sup>);  $\gamma$  is the psychrometric constant (kPa °C<sup>-1</sup>),  $\Delta$  is the slope of the saturation vapor pressure curve (kPa °C<sup>-1</sup>);  $\beta$  is Bowen ratio;  $g_a$  is aerodynamic conductance (m s<sup>-1</sup>);  $\mu$  is wind speed (m s<sup>-1</sup>)), and  $\mu$ \* is friction velocity (m s<sup>-1</sup>).

240 To evaluate differences among years, we first detrended the daily data by subtracting the multi-year average daytime ecosystem respirationseasonal cycle. The resulting anomalies were compared across years using the Kruskal-Wallis test, followed by pairwise Wilcoxon rank-sum tests with Bonferroni correction for multiple comparisons.

We then computed GPP<sub>sut</sub> as GPP at Rg of 1000 W m<sup>-2</sup> and assigned it to the middle of each moving window, as GPP<sub>sut</sub> does not always reflect the light saturation value 2.5 The impact of varying soil moisture conditions

245 To evaluate the influence of soil moisture conditions on ecosystem functioning, we computed the soil saturation ratio (SSR) as the ratio of measured soil water content (SWC) to its 99th percentile across the entire observation period. We then analysed the response of carbon and water fluxes to SSR variability by binning the data into SSR intervals while controlling for the main environmental drivers that could otherwise overshadow the effects of soil moisture variability. Because of the strong seasonality of fluxes and the lack of LAI data, we restricted the analysis to summer months (JJA) to ensure a fully developed canopy.

Canopy photosynthetic capacity (GPP<sub>sat</sub>) was calculated for each 0.1 SSR bin using daytime data from dry- and active-canopy days. This was done both for data pooled across all three summers, to capture the overall response pattern, and separately for each summer to assess interannual variability. Using GPP<sub>sat</sub> rather than GPP allowed the removal of light as the primary driving factor.

255 To control for temperature effects on ER, we initially attempted to obtain ER at fixed temperature by fitting temperature response curves to measured nighttime ER data (nighttime NEE) in SSR bins. However, the range of air temperatures within bins was insufficient. Instead, we used reference ER at 15 °C (ER<sub>ref</sub>) as provided by the ReddyProcWeb partitioning procedure, which allowed the impact of SSR on ER to be analysed independently of air temperature variability.

Because ET is strongly driven by VPD, we divided ET by VPD and calculated mean values for 0.05 SSR bins. To minimise
the influence of evaporation, only half-hourly data from dry- and active-canopy days and under sufficient light conditions were
included. Similarly, EWUE was normalised by daytime VPD before calculating averages for 0.05 SSR bins.

To examine how soil moisture modifies the sensitivity of canopy conductance, Gc was divided into 0.1 SSR bins, using data from all three summers. For each SSR bin, reference canopy conductance (Gc<sub>ref</sub>) was estimated by fitting the Oren et al. (1999) model (Eq. 5):

 $265 \quad G_c = -m \ln(\text{VPD}) + G_{c,\text{ref}} \tag{5}$ 

Where Gc is canopy conductance (mm s<sup>-1</sup>), m is the stomatal sensitivity,  $Gc_{ref}$  is reference canopy conductance at 1 kPa, VPD is vapour pressure deficit (kPa).

Although the slope  $(m/Gc_{ref})$  generally fell within the expected range of 0.5 - 0.7, three SSR classes with low  $R^2$  values (0.05, 0.03) and 0.15) exhibited notably lower slopes (0.23, 0.23) and 0.44, respectively; Table B1, Figure B1). To evaluate whether  $Gc_{ref}$  estimates were biased by poor model fits, we derived an additional set of  $Gc_{ref}$  with fixed  $m/Gc_{ref} = 0.6$  (Figure B2). This approach improved  $R^2$  values, while  $Gc_{ref}$  estimates remained largely unchanged (Table B1). We therefore based subsequent analyses on  $Gc_{ref}$  values calculated with the fixed slope, while also indicating the alternative estimates in Figure 6b. Similar analysis was carried out for each growing season separately to assess the interannual difference in  $Gc_{ref}$  sensitivity to soil moisture variability.

## 275 2.6 Drought recovery and carry-over effects

280

285

290

305

310

315

To disentangle the possible carry-over effects of the drought year from the natural interannual variability, we applied a twostep approach combining model-based analysis of ecosystem fluxes with resistance, recovery and resilience indices. To ensure temporal consistency, we restricted the analysis to a common portion of the growing season (May-September) for each year. First, we assessed whether observed interannual variability in GPP and ER could be attributed solely to changes in their primary environmental drivers (light and temperature, respectively). To do this, we estimated Michaelis-Menten light response curve parameters (Eq. 2) within a running three-day window using half-hourly daytime GPP and Rg data for each year separately. For ER, we utilised ER<sub>ref</sub> and E0 parameters derived during flux partitioning in the ReddyProcWeb tool (Eq. 1). Each year's parameter set was then used to model GPP and ER across all three years using measured Rg and air temperature of each corresponding year. This cross-year modelling allowed us to test whether model parameters obtained for one year could accurately predict flux dynamics in other years. Differences between fluxes when applying parameters from a non-drought year to drought or recovery years (and vice versa) can thus highlight a possible carry-over effect, reflecting changes in ecosystem functioning that persist beyond immediate environmental conditions.

To further quantify the magnitude of the drought impact and evaluate the ecosystem's ability to recover, we calculated resistance (Rt), recovery (Rc), and resilience (Rs) indices for daily carbon exchange components (GPP and ER) and their main driver-normalised versions (GPP<sub>sat</sub> and ER<sub>ref</sub>); daily sums of ET, transpiration (T, estimated as the daily average of ET, filtered to maximise the share of T); EWUE and Gc. For each parameter, daily estimates from May to September were used with 2017 serving as a reference year ("ref"), 2018 as the drought one ("dry") and 2019 as a post-drought recovery year ("rec") (Eq. 6). Resistance (Rt) was calculated as the ratio of daily values during the drought year to those of the reference year, recovery (Rc) as the ratio of recovery to reference year values, and resilience (Rs) as the relative rebound following the drought (Lloret et 295 <u>al., 2011; Portela et al., 2023):</u>

$$Rt = \frac{dry}{ref}$$
;  $Rc = \frac{rec}{ref}$ ;  $Rs = \frac{rec \cdot dry}{ref \cdot dry}$ 

To estimate uncertainty, we applied non-parametric bootstrapping (n = 5000) on daily values, resampling within each year independently. For each index, we report the bootstrapped mean and 95 % confidence intervals.

We acknowledge a limitation in the selection of a single reference year, 2017, which may not fully represent long-term baseline conditions. Consequently, both the magnitude and interpretation of the indices should be viewed in the context of this wet year reference. Additionally, we note that the interpretation of drought-induced changes in EWUE differs from that of other variables. While increases in EWUE may suggest that the ecosystem is coping under stress by maintaining carbon uptake relative to water loss, they often result from stomatal regulation and reduced transpiration, and thus may reflect a physiological stress response rather than enhanced functioning.

-Only the values from windows with significant fit parameters (p<0.05) and R<sup>2</sup>>0.5 were retained. Annual GPP<sub>sat</sub> was then calculated as the 95th percentile of each year's filtered values.

The start and end of each growing season (GS) were estimated using a double-logistic curve fitting method applied to daily GPP sums (Gonsamo et al., 2013). Partial correlation analysis using Spearman's coefficient (rs) was performed to identify the strongest correlation between the fluxes and the primary environmental drivers for each GS. The significance of the difference between GSs was estimated with the Wilcoxon signed rank test using daily values and matching days of the three growing seasons. Each GS was compared to the other two, and a Bonferroni adjustment was applied to the p-values to correct for

Light response curves (Eq. 2) were used for each GS to characterise the impact of global radiation on the daytime net C exchange; the Lloyd and Taylor equation (Eq. 3) was used to assess the ecosystem respiration temperature response. In both cases, we utilised only measured quality-controlled NEE values. All data analysis was performed in MATLAB (2020a-2022b, Mathworks Inc.).

$$NEE_{day} = GPP + ER_{day} = \frac{\alpha GPP_{max}R_g}{\alpha R_g + GPP_{max}} + ER_{day}, \tag{2}$$

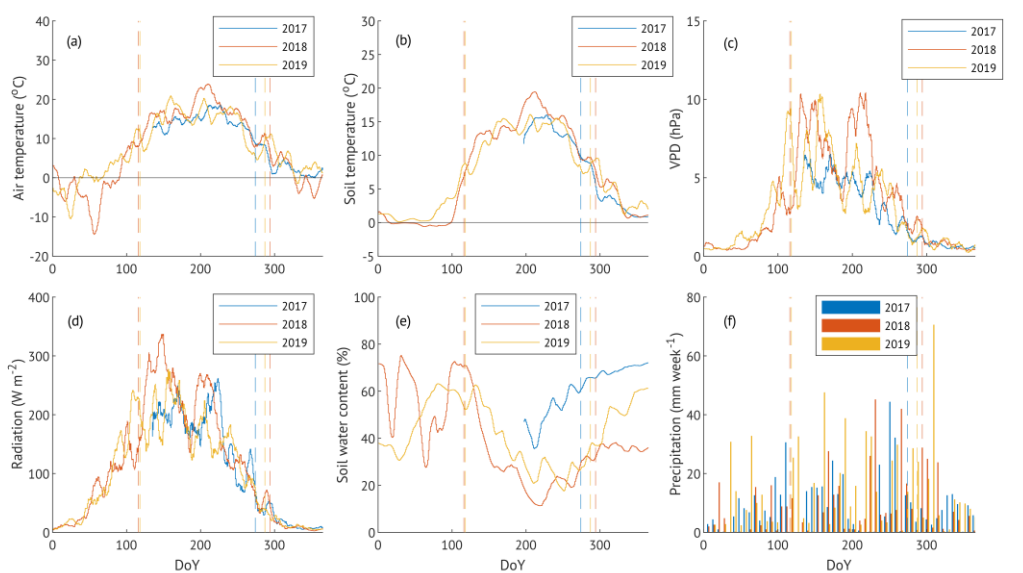
$$ER = ER_{ref} e^{E_0 \left(\frac{1}{T_{ref} - T_0} - \frac{1}{T - T_0}\right)},$$
(3)

where  $R_{ref}$  (µmol m<sup>-2</sup>-s<sup>-1</sup>) is the respiration at the reference temperature; E0 (kJ mol<sup>-1</sup>) is the activation energy; T (°C) is the measured air temperature.  $T_{ref}$  was set to 15 °C, and  $T_0$  was kept constant at -46.02 °C following Lloyd and Taylor (1994).

#### 3. Results

330

## 3.1 Weather conditions



Meteorological conditions and growing season length

325 Figure 2: Climatic conditions during the three studied years: 10-day running means of meteorological parameters (a-e) and weekly sums of precipitation (f). Dashed lines denote the beginning and end of the corresponding growing seasons.

The meteorological conditions of the three studied years (2017-2019) were across the three study years exhibited a strong seasonality typical for the region, with below-zero air temperatures (Ta), reduced vapour pressure deficit (VPD), and low solar radiation during the winter months, and positive air temperatures, higher VPD and increased solar radiation in summer (Fig. 2). The average Ta was similar in 2017 and 2019, whereas the 2018 GS Ta was 1.5 °C higher than the average of the other two years. Likewise, VPD was the highest in GS 2018, while the amount of rain and soil water content were the lowest. (Figure 2). The mean annual air temperature reached the maximum in July; global radiation and VPD demonstrated two distinctive peaks in the beginning and middle of a GS. VPD peaks were absent in 2017; generally, VPD was lower and exhibited less variability in GS 2017 compared in 2017 was close to the subsequent GSs.

335 10-year average (6.6 °C), while both 2018 and 2019 were around 1°C warmer (Table 1). Based on differences in soil water content (SWC)-), we categorised the years as "wet" (2017), "drought" (2018), and "recovery" (2019), reflecting conditions before, during and after a pronounced drought. Although in-situ SWC measurements commencedbegan only in the second part of-mid-July 2017. Data, observations from a nearby station (Appendix Fig. 1Figure C1) and visual assessmentassessments during the installation of the instrumentation confirm increased setup confirmed elevated SWC levels of SWC ((including the installation)).

standing water) also in late spring to and early summer of 2017. SWC exhibited similar patterns in 2018 and 2019, characterized by a rapid decrease at the start of the growing season, reaching the minimum around the beginning of August 2018 (DoY 220) and the end of July 2019 (DoY 209). In both years, this dry period matched the second peaks of solar radiation and VPD, with values in 2018 higher than those in 2019. The end of July was also the driest for 2017, but with still higher SWC levels, lower radiation, air temperature and VPD.

The growing season (GS) length was 179 and 170 days in 2018 and 2019, respectively (the flux measurements of 2017 missed the beginning of the growing season). The start of GS was around a similar time, April 26<sup>th</sup> and April 28<sup>th</sup>, in 2018 and 2019, but the end of GS was later in 2018 (October 21<sup>th</sup>) than in 2019 (October 14<sup>th</sup>) and 2017 (October 1<sup>th</sup>) (Fig. 2).

#### 3.2 Annual and growing season accumulated fluxes

345

360

The riparian alder forest in our study acted as a strong net C sink in all three calendar years (Table 1), with total net C uptake in 2018 being 11% higher than in the previous year and 34 % higher than NEE in the subsequent that year. The difference in C uptake between the 2018 and 2019 was

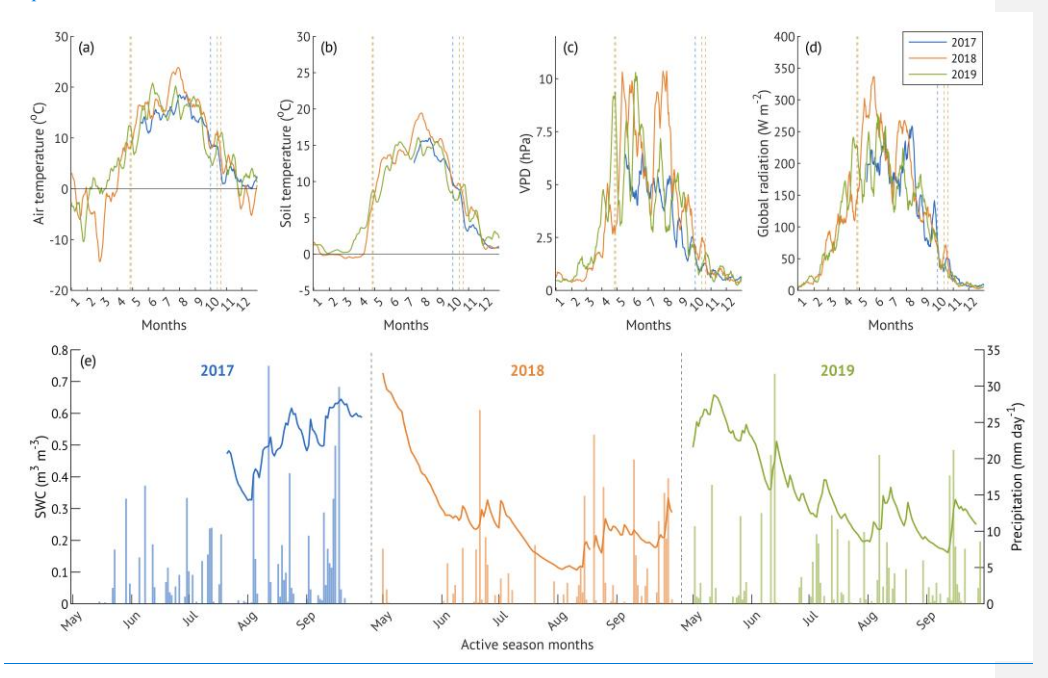


Figure 2: Hydroclimatic conditions during the three studied years (a-d): 10-day running means of meteorological parameters; dashed lines denote the beginning and end of the corresponding growing seasons. Daily soil water content and cumulative daily precipitation (e) of May-September. X-axis ticks correspond to the beginning of each month.

Interannual differences in SWC dynamics during the active vegetation season (May-September, Figure 2e) were primarily driven by ER, which was 36% lower in 2018, while GPP was only 11% lower-precipitation (P) distribution, interacting with the site's dense clayish soils with limited infiltration. In 2017, the rainfall distribution was skewed toward the second part of the season (August-September), resulting in elevated SWC and localised flooding.

In contrast, 2018 experienced extended dry spells in May and July, resulting in a pronounced soil moisture deficit (Figure 2e). SWC declined from 0.73 to 0.28 m<sup>3</sup> m<sup>-3</sup> over 33 days in May (May 1<sup>st</sup> – June 3<sup>rd</sup>, -0.014 m<sup>3</sup> m<sup>-3</sup> day<sup>-1</sup>) and from 0.33 to 0.11 m<sup>3</sup> m<sup>-3</sup> over 32 days in July (July 2<sup>nd</sup> – Aug 3<sup>rd</sup>, -0.007 m<sup>3</sup> m<sup>-3</sup> day<sup>-1</sup>). These periods of progressive drought coincided with

elevated vapour pressure deficit (VPD), and the second part of July to early August period overlapped with a previously identified heatwave period (Krasnova et al., 2022).

365 In 2019, precipitation was more evenly distributed throughout the season, resulting in moderate SWC and intermediate cumulative precipitation (Table 1). Despite the contrasting seasonal patterns, total May-September precipitation across all three years remained within one standard deviation of the 12-year mean (336±75 mm). Although our SWC measurements were limited to the upper soil layer (10 cm depth), the observations remain ecologically meaningful, as alder roots are predominantly confined to shallow depths due to their adaptation to waterlogged, compacted soils.

#### 3.2 Interannual differences in accumulated fluxes

385

Over all three years of the study, the alder forest acted as a strong net carbon sink (annual NEE < 0) (Table 1). Accumulated NEE in the active vegetation season (May-September) accounted for 9796% of the total annual flux (97% in 2018 and 95% in 2019. Using an average of 96%;). Based on this seasonal share, we estimated the total annual NEE for 2017 to be -599.6600 g C m<sup>-2</sup> y<sup>-1</sup>, reflecting a smaller C-uptake than in 2018, but higher than in 2019. In a similar manner Following the same approach, we obtained estimates for annual GPP in 2017 (May—September GPP was onalso accounting for an average of 96% of the total), and then estimated accumulated subsequently calculated ER as athe difference between GPP and NEE. Similarly, as the majority of evapotranspiration (ET) occurred during the active season (94% in 2018 and 91% in 2019), total annual ET and ecosystem water use efficiency (EWUE; GPP. The average/ET) were estimated for 2017. Across the study period, the three-year means (±SD) for annual NEE, GPP-and, ER over the three years of our study was, and ET were -586.3 ± 84.5, -1329.8 ± 85, -1330 ± 82.4 and 742.9, 743 ± 166.3 g C m<sup>-2</sup> y<sup>-1</sup> and 264 ± 74 mm y<sup>-1</sup>, respectively. The net C uptake in 2018 was 21% higher than the average of the other two years, while GPP and ER were 8% and 27% lower.

Total evapotranspiration (ET) in 2018 was almost twice lower (43%) than the 2019 value. Consequently, the annual EWUE 2018 was 55% higher than in the following year. The majority of the total ET occurred during May September (94% in 2018 and 91% in 2019), allowing for an estimate of total ET and EWUE in 2017 (Table 1). The average annual ET over the three years was  $263.6 \pm 74.5$  mm  $y^+$  and annual EWUE averaged to  $5.27 \pm 1.16$  g C kg H<sub>2</sub>O<sup>+</sup>; annual ET and EWUE in 2018 were 35% lower and 40% higher than the average of the two other years, respectively.

Table 1. Average meteorological parameters (mean and standard deviation) and aggregated fluxes over the measurement years and active vegetation season (May to September)

Table 1. Annual and May-September average air temperature (Ta), soil temperature at 10 cm depth (Ts), global radiation (Rg), soil water content at 10cm depth (SWC); Annual sums of precipitation (P), net ecosystem exchange (NEE), gross primary production (GPP), ecosystem respiration (ER) and evapotranspiration (ET), ecosystem water use efficiency (EWUE) in the wet (2017), dry (2018) and recovery (2019) years. The May-September values are shown inside parentheses. EWUE was calculated from the sums of GPP and ET of the corresponding periods.

	Ta	Ts	Rg	VPD	SWC	Prec.	NEE	GPP	ER	ET	EWU
											E
	<u>Ta</u>	Ts	Rg	VPD	SWC	<u>P</u>	NEE	GPP	ER	ET	EWU
≒I	$^{\circ}C$	$^{\circ}C$	$W m^{-2}$	hPa	$m^3 m^{-3}$	mm period	g C m <sup>-2</sup>	g C m <sup>-2</sup>	g C m <sup>-2</sup>	mm	<u>E</u>
Year						1	period-1	period <sup>-1</sup>	period <sup>-1</sup>	period <sup>-1</sup>	g C kg
											$H_2O^{-l}$
Calend	<del>dar year</del>										
2017							<del>-599.6</del>	-1310.7	711.1	255.1	5.1
2018	$7.6 \pm 10.6$	$7.5 \pm 6.8$	<del>113.7 ±</del>	$3.4 \pm 4.9$	$0.39 \pm 0.19$	4 <del>52.6</del>	-663.4	-1258.2	594.9	193.7	6.5
			200.8								
2019	$7.7 \pm 8.5$	$7.4 \pm 5.7$	<del>102.5 ±</del>	$3.1\pm4.3$	$0.43 \pm 0.14$	710.0	<del>-495.9</del>	<del>-1419.8</del>	922.8	342.0	4.2
			<del>182.6</del>								
May-S	<del>leptember</del>										

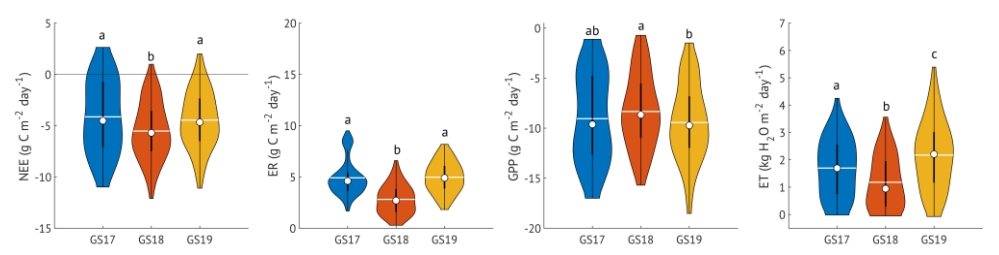
2017	<u>6.4*</u> (14.5	<u>(</u> 13.8—±	<del>173.5 ±</del>	<u>(</u> 4.2 <del>_±</del>	<u>(</u> 0.52—±	<del>239.8</del> 690	<del>-575.6</del> 600	- <u>1311 (-</u>	<del>682.7</del> 711	<u>255</u>	5.1
	±4.2)	1.8* <u>)</u>	<del>229.4</del> -(174)	<del>3.5</del> )	0.09***)	(372)	<u>(-576)</u>	1258 <del>.3</del> )	(683)	(236 <del>.0</del> )	(5.3)
2018	<u>7.6 (</u> 16.9 <del>±</del>	<u>7.5 (</u> 14.6±	<u>114 (</u> 204 <del>.2 ±</del>	<u>3.4</u> (6.5	<u>0.39 (</u> 0.28 ±	<del>241.4</del> 518	<del>-775.5</del> 663	-1258 (-	4 <del>39.5</del> <u>595</u>	<u>194</u>	6.5
	<del>5.6</del> )	<del>2.8</del> )	<del>253.7</del> )	± 6.1)	0.14)	(271)	<u>(-776)</u>	1215 <del>.0</del> )	(440)	(182 <del>.3</del> )	<b>(</b> 6.7 <b>)</b>
2019	<u>7.7 (</u> 14.8 <del>±</del>	<u>7.4 (</u> 13.1±	<del>167.8 ±</del>	<u>3.1 (</u> 5.0	<u>0.43 (</u> 0.36 ±	<del>376.4</del> 665	<del>-634.9</del> 496	<u>-1420 (-</u>	923	<del>311.7</del> <u>34</u>	<u>4.2</u>
	<del>5.8</del> )	<del>2.7</del> )	<del>220.4</del> 103	± 5.0)	0.14)	(338)	<u>(-635)</u>	1351.4)	<u>(715.4)</u>	2 (312)	<u>(</u> 4.3 <u>)</u>
			<u>(168)</u>								

<sup>\*</sup>data from the Estonian National Weather Service;

\*\* starting from 24.07.2017

400

405

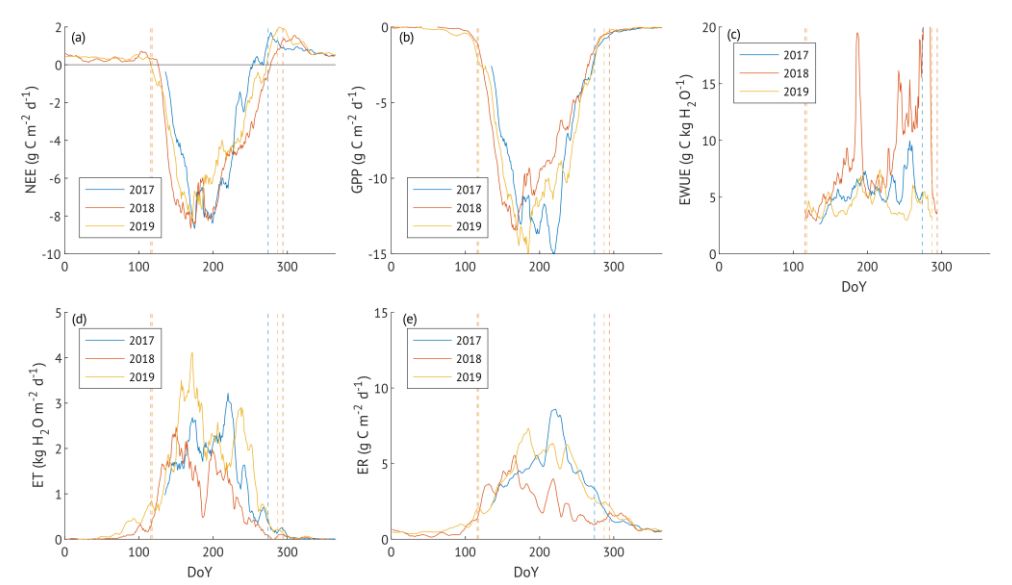


Total GPP in the active vegetation season of 2018 was only 3% lower than the previous year but 10% lower than the following year. Total ER over May September varied between the years, with the lowest aggregated C release in 2018 (39% lower than in 2019 and 36% lower than in 2017). Total ET was also the smallest in 2018 (42% lower than 2019 and 23% lower than 2017). Similar to the annual EWUE dynamics, active vegetation season EWUE was the highest in 2018, followed by a 36% decrease in the following year. ET to precipitation ratio was 0.98, 0.76, 0.83, in May September of the three studied years, respectively.

Figure 3: Violin plots of carbon and water fluxes over the three studied growing seasons. Markers are median values, and white horizontal lines denote averages. Colours denote growing seasons of different years. Matching letters mark no statistically significant difference between the medians (Wilcoxon signed-rank test p>0.05, Appendix table 1)

Daily NEE during the GS exhibited the highest net C uptake rate in 2018 (Fig. 3), while no significant difference was observed between daily NEE in 2017 and 2019 (p = 0.2). Daily ER in GS2018 was significantly reduced compared to both other years; daily GPP in GS2018 was similar to the previous GS but smaller than the following year's GS. ET across all three GSs differed significantly, with the highest ET recorded in 2019 and the lowest in 2018, resulting in the highest total EWUE in GS2018 (Table 1).

3.3-The net carbon uptake of the 2018 drought year was highest among the three years, with May-September NEE exhibiting a 35% increase relative to the wet year 2017 (p<0.001). This enhanced net sink was a result of a significant and strong reduction



in ER (-36%, p<0.001), while GPP declined only marginally (-3.4%, p>0.1). In the recovery year (2019), NEE during the active season was 18% lower than in the drought year (p<0.001) yet remained 10% higher than in the wet year (p=0.02). ER featured the highest difference, significantly increasing by 62.5% (p<0.0001) relative to 2018, but exceeding 2017 values only by 4.7% with no difference between the daily values of the active season (p>0.1). GPP also increased in 2019, though mildly, with values 11% higher than in the drought year (p=0.0004) and 7.4% above those of the wet year (not significant).

Total evapotranspiration (ET) of the drought year active season significantly decreased by 23% compared to 2017. ET in the recovery year was the highest of the three years, increasing by 71% compared to the drought year and 32% compared to the wet year. The difference between the daily values in all three study years was significant (p<0.001). The active season share of ET in P (ET/P) was the same in wet and dry years (0.69 and 0.67, respectively), while noticeably increasing in the recovery year (0.92). EWUE (calculated as GPP/ET) peaked in the drought year, when carbon uptake remained relatively stable despite limited water loss, and was lowest in the recovery year, both annually and for the active vegetation period (May-September) (Table 1).

425

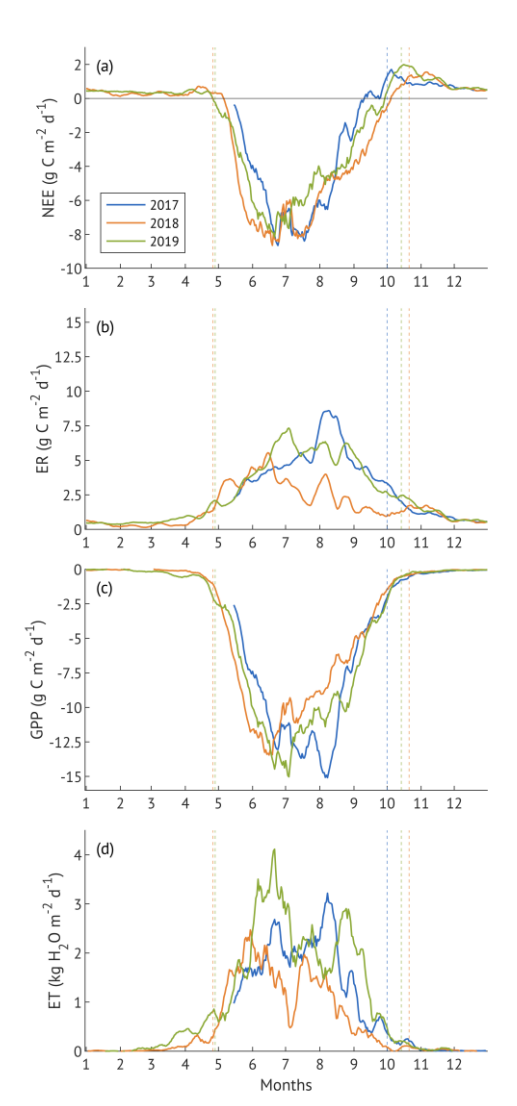


Figure 3: Seasonal dynamics of net ecosystem exchange (NEE, a), ecosystem respiration (ER, b), gross primary production (GPP, c), evapotranspiration (ET, d) represented by 10-day running means. Vertical dashed lines are the borders of growing seasons. X-axis ticks correspond to the beginning of each month.

#### 3.3 Seasonal dynamics of carbon and water exchange

Figure 4: Seasonal dynamics of net ecosystem exchange (NEE, a), gross primary production (GPP, b), ecosystem water use efficiency (EWUE, c), evapotranspiration (ET, d), ecosystem respiration (ER, e), and represented by 10 days running means. Vertical dashed lines are the borders of growing seasons (GS). EWUE was calculated from 10 days running means of GPP and ET.

In all three study years, daily NEE was positive (net C release) during the late autumn, winter and early spring and predominantly negative (net C uptake) from the end of April — beginning of May (Fig. 4a). NEE peaked around the second part of June, followed by a slight decrease in sink strength and a second peak around mid July, observed in 2017 and 2018, but not in 2019. Daily NEE reached —8.9,—8.8 and —7.4 g C m<sup>-2</sup> d<sup>+</sup> in 2017-2019, respectively. The ecosystem transitioned to a consistent net C source by mid-September 2017 and by the end of September 2019. In 2018, NEE remained negative for the longest period, reaching positive values only in early October. The autumn months were characterised by net C release reaching 1.3, 1.4 and 1.7 g C m<sup>-2</sup> d<sup>+</sup> in the three study years, respectively.

The seasonal cycle of ER varied across all three years (Fig. 4e), reaching its maximum in the early part of August 2017 (8.3 g C m $^2$  d $^4$ ) and the latter part of June 2019 (6.9 g C m $^2$  d $^4$ ). In 2018, the initial increase of ER that peaked at 4.5 g C m $^2$  d $^4$  in the beginning of summer was followed by a rapid decrease mid-June and significantly (p<0.0001) lower values throughout the entire GS.

The GPP seasonal dynamics was more consistent between 2018 and 2019, with the peak occurring mid-June 2018 and in the beginning of July 2019 (Fig. 4b). However, absolute GPP values were smaller at the start of GS2019 and higher throughout most of the GS compared to the previous year. The GPP dynamics in 2017 differed from the two subsequent years, starting with lower absolute values but becoming more prominent in the second half of GS, peaking later in the first part of August. The highest C uptake was 14.6, 12.8 and 13.5 g C m<sup>2</sup> d<sup>+</sup>in 2017-2019, respectively.

The ET seasonal cycle exhibited a clear pattern with low values outside the GS and two distinctive peaks during the GS of all the years; however, their height, timing, and the dip between them varied considerably (Fig. 4d). ET reached maximum of 3.1 kg H<sub>2</sub>O m<sup>2</sup> d<sup>+</sup> in the beginning of August 2017; the highest ET of 2018 was in the end of May beginning of June (2.4 kg H<sub>2</sub>O m<sup>2</sup> d<sup>+</sup>), and the 2019 ET peaked the most in the end of June beginning of July (3.5 kg H<sub>2</sub>O m<sup>2</sup> d<sup>+</sup>). fluxes, and canopy physiologicalEWUE reached its highest values in 2018, marked by a notable peak in the beginning of July and substantially

470 higher values in the second part of GS compared to other years (Fig. 4c). EWUE varied the most in 2018 (CV=2.02), followed by 2017 (CV=0.25) and 2019 (CV=0.23).

#### 3.4 The impact of environmental drivers on carbon and water fluxes

475

Across the GSs of all three studied years, water and C fluxes increased with air temperature, although the shape of response curves varied (Fig. 5 a1 — a4). In 2017 and 2019, NEE and GPP displayed similar patterns with no impact (NEE) or slight increase (GPP) with air temperature up to around 10 °C, followed by a sharper rise and a saturation at approximately 22 °C. In 2018, GPP reached the saturation point earlier (19°C) and exhibited no further impact until 27 °C, after which it was slightly reduced. Generally, GPP, ER and ET had lower values across all air temperature bins in 2018. More negative NEE at lower air temperatures in 2017 was caused by increased GPP compared to other years, while ER was similar to 2019. ET at lower temperatures was higher in 2017 compared to the other two years. The 480 correlation between the C and water exchange and the air temperature was significant in most of the years, except for ER in GS2017, when soil temperature was indicated as the main factor, and ET when the air temperature effect was overshadowed by the leading influence of radiation (Appendix table 2). parameters

Atmospheric dryness demonstrated a saturating effect on NEE, caused by GPP saturation at VPD around 7-8 hPa for all the years, although 2018 GPP was lower across most bins. Due to the non-monotonic nature of VPD impact on GPP (the decrease after the plateau at around 14 hPa), rs was very low or not significant (Appendix table 2). ER increased with VPD in 2018, 485 likely due to its connection with temperature, while no impact of VPD on ER was observed in 2017 or 2019. A similar, although less sharp, saturating effect of VPD was observed for ET, with 2017 and 2019 exhibiting almost identical curves; the 2018 VPD response curve was lower and flatter. VPD was the second most important environmental driver for ET (after Rg) in all years (r, ranging from 0.30 to 0.45) and the most important when the Rg was considered as a fixed factor (r, 0.37-Carbon exchange components (NEE, GPP, ER) and ET exhibited distinct seasonal patterns in all years, with a sharp increase in spring, peak rates around mid-summer, and a decline toward autumn, reflecting the typical phenological cycle of a deciduous forest in the hemiboreal zone (Figure 2). However, the timing, magnitude and duration of flux peaks varied among the study years. In the "wet" year 2017, relatively cool spring and summer temperatures (Figure 2) delayed the onset of ER, GPP and ET (Figure 3b-d), all of which increased more gradually compared to 2018 and 2019. Persistently high SWC supported elevated 495 ET throughout the season, but lower VPD limited evaporative demand, resulting in lower ET rates than observed in the recovery year. All three fluxes peaked in August, following a period of warmer temperatures and clear-sky conditions, with ET exceeding the recovery year levels. A prolonged increase in ER during September-October contributed to an earlier decline in net carbon uptake (NEE) relative to the other years (Figure 3a).

In contrast, the 2018 drought year was characterised by higher spring and summer air and soil temperatures, elevated VPD, and a progressive decline in SWC, particularly in May and again from July onward. These conditions contributed to an earlier rise in ER, GPP and ET, followed by a sharp suppression of all fluxes once SWC became limiting. Despite high atmospheric demand, ET noticeably declined in July and August, consistent with water limitation. ER was more strongly suppressed than GPP in late summer, leading to a more negative NEE and thus enhanced net carbon uptake toward the end of the growing

In the recovery year 2019, spring conditions resembled those of 2018, but less extreme heat and more even precipitation 505 distribution prevented soil moisture depletion. Warm summer with peaking air temperatures in June supported earlier peaks in ER and GPP, with cooler and wetter conditions in July and August co-occurring with a moderate decline in both fluxes. ET exhibited two distinct peaks, in June and again in August-September, and remained almost consistently higher than in the other two years, supported by moderate VPD, ample SWC, and frequent rainfall events.

510 The seasonal dynamics of ER and GPP are strongly governed by their main environmental drivers, temperature and light, respectively. Moreover, daytime ER is modelled based on temperature, which can bias direct comparisons across years. Therefore, ER<sub>ref</sub> (ER at reference temperature) and GPP<sub>sat</sub> (canopy photosynthetic capacity, i.e. GPP at saturating light) are more objective measures for evaluating interannual differences in seasonal variability (Figure 4).

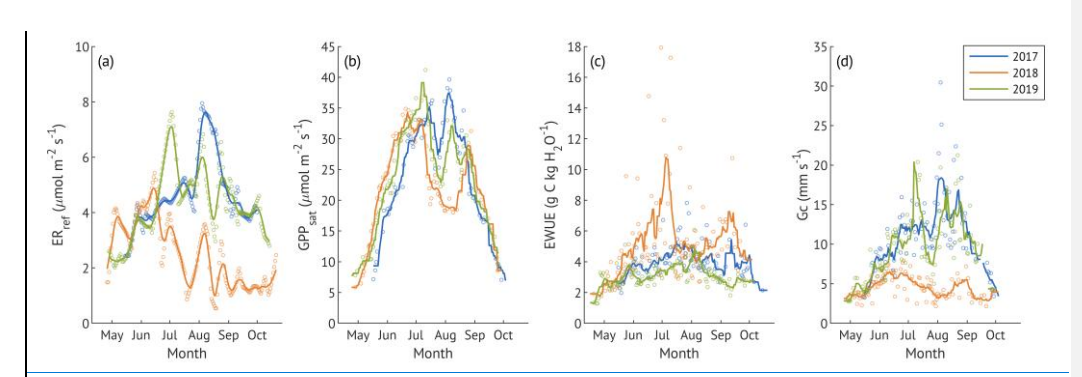


Figure 4: Seasonal dynamics of reference ecosystem respiration (ERref, a) and canopy physiological response parameters: canopy photosynthetic capacity (GPPsat, b), water use efficiency (EWUE, c), and canopy conductance (Gc, c). Lines denote 10-day running means. X-axis ticks correspond to the beginning of each month. EWUE markers are daily values that were calculated from sums of GPP and ET filtered for the active photosynthesis and transpiration under sufficient light (Rg > 435 W m²). GPPsat makers are the centres of 3-day running windows. Gc markers are the daily average values from the half-hourly estimates under sufficient light.
 All canopy parameters were obtained only for the days with < 1mm of rain, GPP > 1 g C m² d¹ and ET > 0.25 mm d⁻¹ for three growing seasons.

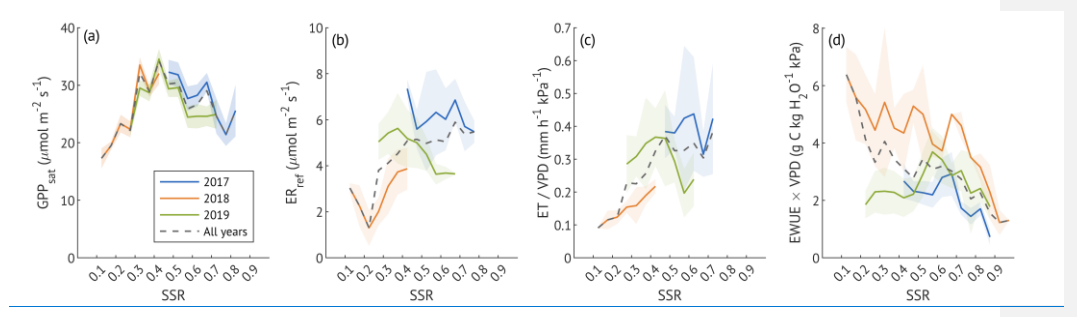
ER<sub>ref</sub> exhibited clear seasonal patterns across three years, with distinct peaks in August 2017, May 2018, and June 2019 (Figure 4a). The severe suppression of ER<sub>ref</sub> from June to October 2018 confirms that factors beyond temperature strongly influenced ecosystem respiration during the drought year. In contrast, 2017 and 2019 maintained more consistent ER<sub>ref</sub> during the growing season. Average ER<sub>ref</sub> were  $4.7 \pm 1.3$ ,  $2.5 \pm 1.2$  and  $4.3 \pm 1.3$  µmol m<sup>-2</sup> s<sup>-1</sup> in 2017-2019, respectively, with no significant difference detected between the wet and recovery years (p=0.7).

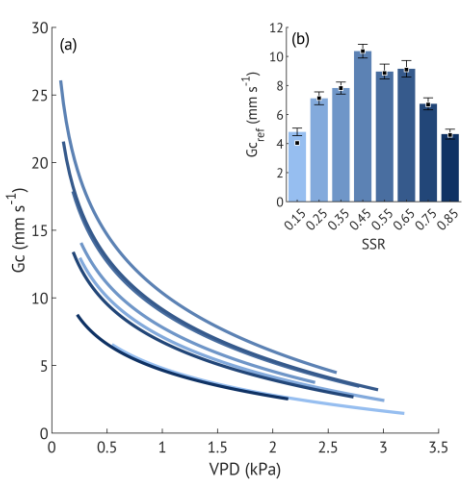
GPP<sub>sat</sub> exhibited a distinct seasonal cycle in all three years (Figure 4b), peaking in June and followed by a sharp mid-summer decline coinciding with VPD peaks (Figure 2c). GPP<sub>sat</sub> in 2018 was elevated during May and early June compared to the other years, but the typical late-summer rebound observed in 2017 and 2019 was absent. Despite these seasonal differences, the average values were  $24.9 \pm 9.1$ ,  $22.4 \pm 7.5$  and  $23.5 \pm 8.2$  µmol m<sup>-2</sup> s<sup>-1</sup> in 2017, 2018, and 2019, respectively, and no significant interannual difference was found (p>0.1). Canopy EWUE varied between the years (Figure 4c), with the drought year demonstrating higher and more variable values ( $5.2 \pm 2.9$  g C kg H<sub>2</sub>O<sup>-1</sup>) than both 2017 ( $4.1 \pm 1.0$  g C kg H<sub>2</sub>O<sup>-1</sup>) and 2019 ( $3.2 \pm 0.7$  g C kg H<sub>2</sub>O<sup>-1</sup>) and noticeably peaking in July and September 2018. The difference between all three years was significant (p>0.1).

530

Canopy conductance (Ge) followed a distinct seasonal pattern in the wet and recovery years, with higher values during summer relative to early and late in the growing season (Figure 4c). Nevertheless, the difference between 2017 and 2019 was significant (p=0.0019), with the recovery year exhibiting a smaller average Gc (9.5 ± 4.4 mm s<sup>-1</sup>) compared to the wet 2017 year (11.1 ± 4.9 mm s<sup>-1</sup>). In contrast, the drought year showed persistently suppressed Gc throughout the season, averaging 4.6 ± 1.4 mm s<sup>-1</sup>, significantly lower than both other years (p<0.001).</p>

#### 40 3.4 The impact of soil moisture variability





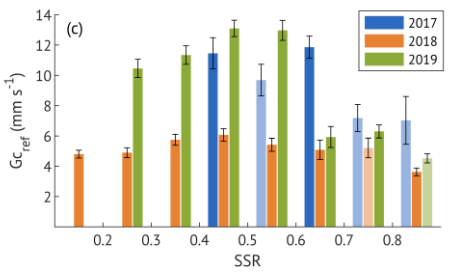


Figure 6: (a) Sensitivity of canopy conductance (Gc) to vapour pressure deficit (VPD) across different soil saturation ratio (SSR) classes, indicated by shades of blue, with darker colours representing higher SSR. Curves represent the Oren et al. (1999) model (Eq. 5) with a fixed slope of 0.6. (b) Reference canopy conductance (Gcref) for each SSR class, where SSR values denote the midpoint of each 0.1 interval. Error bars represent 95 % confidence intervals. Squares indicate Gcref estimates derived from the variable-slope model (see Appendix B for more details). (c) Estimated Gcref per SSR class for each study year, Bars with lighter shading indicate lower quality model fits (R<sup>2</sup> < 0.2). Error bars represent 95 % confidence intervals.

Figure 5: The variation of canopy photosynthetic capacity (GPPsat, a), reference ecosystem respiration (ERref, b), normalised canopy evapotranspiration (ET/VPD, c) and normalised water use efficiency (EWUE × VPD, d) under different soil saturation ratios (SSR) in summer months (JJA) of three study years, GPPsat (a) is shown as the value estimated for each SSR class and year; shaded areas represent the 95% confidence intervals. Other parameters (panels b—d) are shown as averages within 0.05 SSR bins; shaded areas denote ±1 standard deviation. Dashed lines in all panels indicate results for all data pooled across years. For details on data filtering and calculations, see the corresponding section of the Methods.

Over the three contrasting summers, only the data from the recovery year (2019) covered the majority of soil saturation ratio classes (SSR, SWC normalised to the 99th percentile), with the very dry class occurring only in the drought year 2018 (Figure 5). GPP<sub>sat</sub> demonstrated an optimum at 40-50% saturation, declining at both lower and higher SSR. ER<sub>ref</sub> generally increased from low to medium SSR and plateaued thereafter, although in the wet year (2017), ER<sub>ref</sub> remained higher at high SSR compared to the recovery year.

Because both ET and EWUE are strongly influenced by VPD, we normalised them to isolate soil moisture effects (Figure 5c-d). ET increased with SSR, peaking at ~50% before stabilising, resembling the ER<sub>ref</sub> pattern. In contrast, VPD-normalised EWUE declined with increasing SSR, but with distinct interannual differences. In 2017, EWUE remained low and stable at moderate saturation, decreasing further only from 70% saturation. In 2018, EWUE was elevated across most SSR classes, with only minor declines from 10% to 80% and a drop near full saturation. The recovery year (2019) showed an optimum-shaped response, with low

EWUE at 20-50%, a moderate rise at 60%, and a decline at higher SSR.

To examine stomatal regulation under varying soil moisture conditions, we assessed the response of Gc to VPD across the SSR classes, both for all three growing seasons combined (Figure 6a-b) and for each year separately (Figure 6c). Reference Gc (Gc<sub>ref</sub>, canopy conductance at 1 kPa VPD) was the highest at moderate saturation (45%) and the lowest at the driest (15%) and wettest (85%) conditions when data from all years were pooled. This optimum-like pattern was also evident in the wet and recovery years analysed separately. In contrast, during the drought year (2018), Gc<sub>ref</sub> remained low across all SSR classes, with only a slight, non-significant increase at 35–55%. Overall, Gc<sub>ref</sub> in 2018 was about half the magnitude observed in the wet and recovery years at low to medium SSR, coming close to recovery-year values only at SSR ≥65%, when the Gc<sub>ref</sub> of the other 2 years was suppressed.

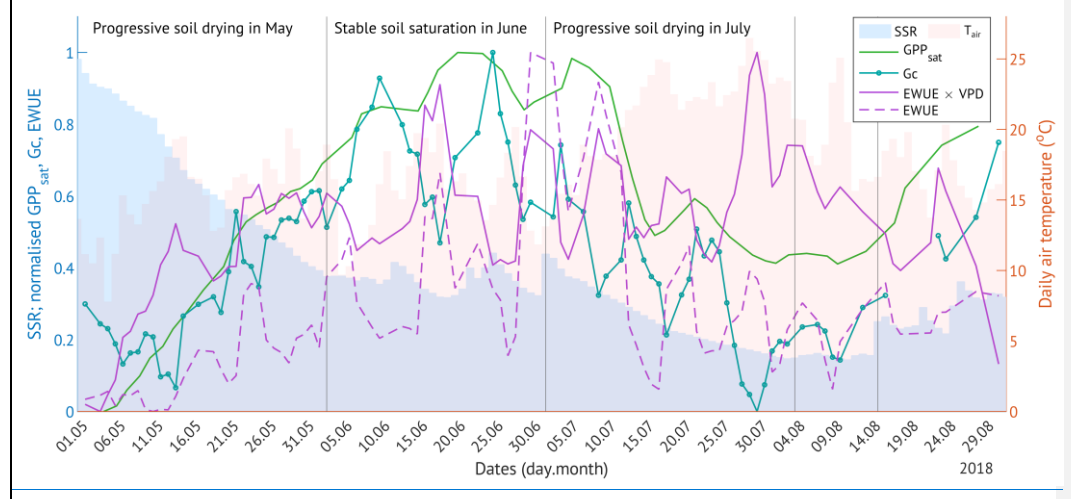


Figure 7: The change in canopy physiological response parameters (photosynthetic capacity, GPPsat; canopy conductance, Gc; water use efficiency, EWUE) with the progressive soil drying in 2018. Shaded bars are the daily soil saturation ratio (SSR, blue) and the daily air temperature (red). All other values are normalised 3-day running means.

In May and July 2018, the forest under study experienced a progressive drought, with soil moisture steadily declining in the absence of rainfall over multiple consecutive days (Figure 7). SSR decreased from full saturation in early May to 37% by the end of the month, remained between 30–50% in June, and dropped further to 15% over July, persisting at low levels through mid-August (Figure 7). While the soil was drying in May, all canopy physiological response variables increased, with maximum values reached under moderate SSRs in June. During the progressive drought in July, most variables declined, with the exception of VPD-normalised EWUE, which reached its highest values under the driest conditions. In early August, when SSR remained at its minimum, GPP<sub>sat</sub> stabilised at approximately half of its June peak, while VPD-normalised EWUE fell from 75% to 45% of its maximum.

#### 3.5 Drought recovery

600

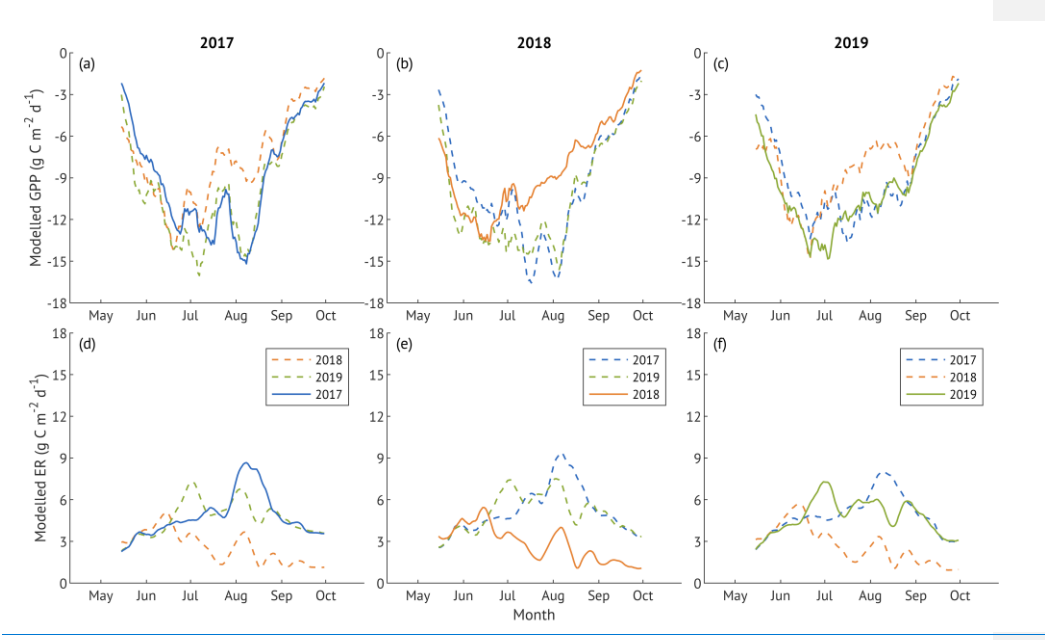


Figure 8. Modelled gross primary production (GPP; panels a-c) and ecosystem respiration (ER; panels d-f) during the growing seasons of 2017 (a, d), 2018 (b, e), and 2019 (c, f). For each year, fluxes were modelled using global radiation (for GPP) or air temperature (for ER) data from the same year with parameter sets derived from the corresponding year itself (solid lines) and other study years (dashed lines). All lines represent 10-day running means.

In the drought year 2018, GPP was reduced from July onwards, a pattern that was not present in 2017 and 2019 (Figure 8a-c). When applying the 2018 model parameters to wet and recovery year radiation data, this GPP suppression persisted. The difference between the observed GPP and modelled values using parameters of other years was significant (p < 0.001), however, most of the difference between wet and recovery years occurred early in the growing season, with matching GPP dynamics in the latter half. On the other hand, no significant difference (p > 0.1) between observed daily ER in 2017 and values modelled using 2019 parameters was found (Figure 8d-f). In contrast, the ER modelled with drought-year parameters was significantly lower than observed fluxes across all years (p < 0.001).</li>

To quantify the drought impact and recovery, we estimated resistance (Rt), recovery (Rt) and resilience (Rs) indices (Figure 9). Based on overlapping confidence intervals, no significant differences were detected between carbon fluxes and their drivernormalised versions (GPP vs. GPPsat; ER vs. ERref) for any of the indices.

The ecosystem's resistance (Rt) to drought exhibited considerable variation among carbon, water, and physiological fluxes.

Carbon uptake (GPP and GPP<sub>sat</sub>) maintained moderate resistance (0.84 and 0.88, respectively), indicating partial but not complete suppression during the 2018 drought. However, the resistance of respiratory fluxes (ER and ER<sub>ref</sub>) was significantly lower (0.57 and 0.53, respectively). Water fluxes, evapotranspiration (ETtot, total ecosystem water loss per day) and transpiration (T, estimated as the daily average of filtered ET with the maximum proportional contribution of water loss) were

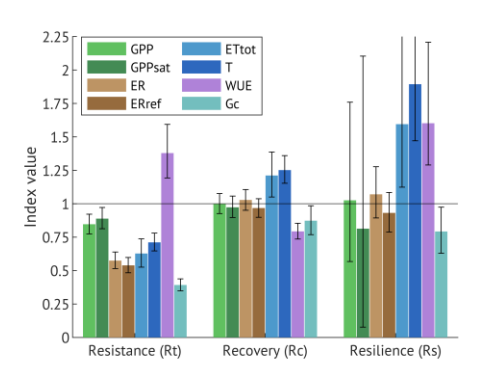


Figure 9. Resistance (Rt), recovery (Rc) and resilience (Rs) indices of the gross primary production (GPP), canopy photosynthetic capacity (GPPsat), ecosystem respiration (ER), reference ecosystem respiration (ERref), evapotranspiration (ETtot), transpiration (T, calculated as filtered ET with maximum share of T), canopy water use efficiency (EWUE) and canopy conductance (Gc). Error bars are 95% confidence intervals.

likewise reduced (0.63 and 0.71, respectively). EWUE exhibited the highest resistance ( $\sim$ 1.38), and Gc was most affected, with Rt = 0.39.

Recovery (Rc) metrics indicated a generally strong rebound in the year following drought (2019), with carbon and water fluxes returning to or exceeding pre-drought levels observed in 2017, and EWUE declining to even lower levels (Rc = 0.79), indicating a return to more "comfortable" conditions. However, Gc recovered only partially (Rc = 0.87).

Resilience (Rs), quantifying the relative recovery magnitude, was generally strong for carbon and water fluxes (Rs  $\geq$ 1), but lower for Gc (Rs = 0.79), which may modulate ecosystem responses to future stress events.



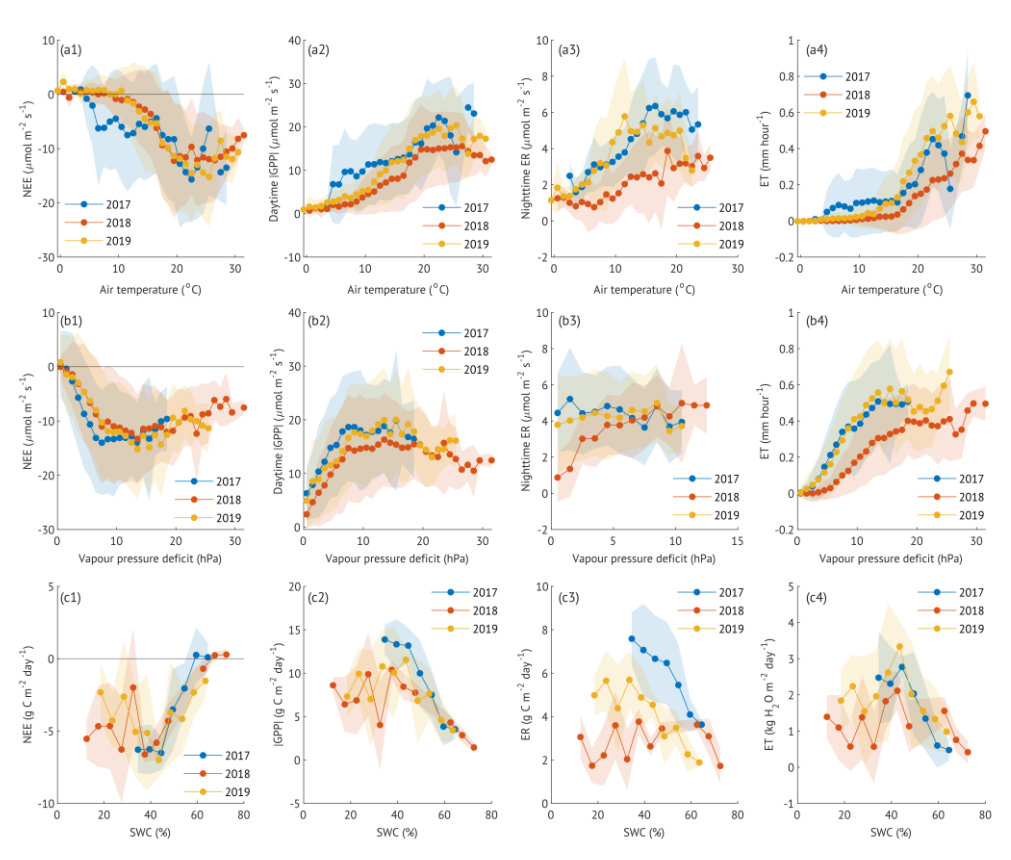


Figure 5: The influence of air temperature (a1-a4) and vapour pressure deficit (VPD, b1-b4) at a half-hourly scale and soil water content (SWC, c1-c4) at daily scale on carbon and water fluxes in 2017-2019 growing seasons. The absolute values of GPP are used in a2, b2 and c2 for convenience. Markers represent the averages of 1 °C / 1 hPa / 5% bins of Tair, VPD and SWC, respectively. Shaded areas denote the standard deviation.

Both NEE and ET reached an optimum at around 40% of SWC. Lower SWC resulted in high variability of NEE stemming from the differences in ER, while GPP in 2018 and 2019 was similar under these lower SWC conditions). SWC was identified as the leading driver for GPP in each GS when the impact of Rg was controlled for  $(r_s = 0.34 \dots 0.51)$ .

Table 2. Parameters of light and temperature response curves (estimates and standard errors per growing season)

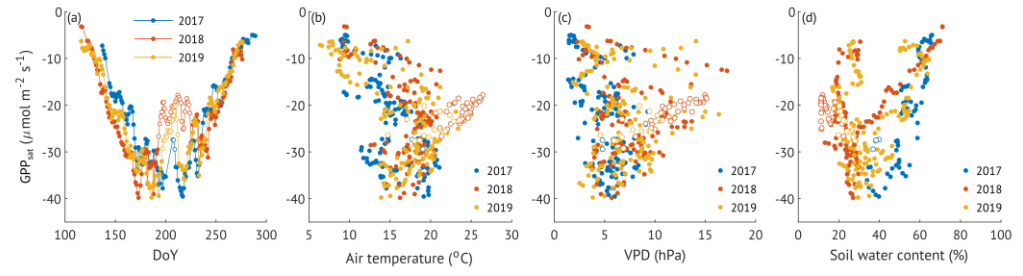
<b>Growing seasons</b>	æ	GPP <sub>max</sub>	ER <sub>day</sub>	$\mathbb{R}^2$	ER <sub>10</sub>	$\mathbb{R}^2$
	μmol J <sup>-1</sup>	$\mu$ mol m <sup>-2</sup> s <sup>-1</sup>	$\mu$ mol m <sup>-2</sup> s <sup>-1</sup>		$\mu mol m^{-2} s^{-1}$	
2017	$0.12 \pm 0.01$	$-28.68 \pm 0.69$	$3.24 \pm 0.61$	0.44	$2.08 \pm 0.13$	0.43
2018	$0.08 \pm 0.01$	$-28.65 \pm 0.76$	$3.16 \pm 0.42$	0.46	$\underline{2.19 \pm 0.07}$	0.11
<del>2019</del>	$0.15 \pm 0.01$	$-26.58 \pm 0.50$	$4.38 \pm 0.56$	0.47	$3.01 \pm 0.09$	0.24

The response of GPP to Rg over all three GSs was consistent, with 2017 and 2018 exhibiting similar light response curve parameters. The GS of 2019, however, demonstrated a slightly lower maximum GPP (GPP<sub>max</sub>) and higher daytime ER (ER<sub>day</sub>). ER<sub>10</sub> had a similar pattern with the highest value occurring in 2019.

#### 3.5 Photosynthetic capacity and water use efficiency

660

The annual canopy photosynthetic capacity (GPP<sub>sat</sub>) was -36.94, 34.77, 36.44 µmol m<sup>-2</sup> s<sup>-1</sup> in 2017-2019, respectively. GPP<sub>sat</sub> exhibited a sharp increase with the highest absolute values at by the end of May—beginning of June (DoY 173-190) followed by a midsummer reduction in the second part of July—beginning of August, observed in all the years (DoY 192-225, Fig. 6a), however it much shorter in 2017. GPP<sub>sat</sub> was steadily decreasing from the end of August. While the spring 2017 had lower GPP<sub>sat</sub> and not so pronounced depression, no significant difference was found in GPP<sub>sat</sub> between the GSs of the three studied years (Appendix table 1).



655 Figure 6: Seasonal cycle (a) of and environmental drivers' influence (b-d) on GPP<sub>sat</sub> during the three measurement years. White markers denote the midsummer GPP<sub>sat</sub> reduction in all sub-figures

Midsummer reduction of GPP<sub>sar</sub> in 2018 was accompanied by increased air temperature (period average and standard deviation: 23.9±1.5 °C), high VPD (12.1±1.2 hPa) and very low SWC (14.4±3.4%) (Fig. 6b-d). A shorter reduction period in 2019 had moderate to high air temperatures (20.0±2.4°C), moderate VPD (8.0±1.8 hPa) and decreased SWC (24.3±3.3%). Only three 5-days periods in 2017 featured significant light response curve fits with reduced GPP<sub>sat</sub>. They were characterised by moderate air temperature (18.4±0.7°C), low VPD (5.1±0.6 hPa) and moderate SWC (38.3±1.5%).

Daily values of EWUE varied greatly with single outstanding values corresponding to high VPD and moderate air temperature. In 2018, EWUE was heightened at lower VPD values compared to other years. Partial correlation analysis (Appendix table 2) also identified VPD as the main driver ( $\rho = 0.36...-0.56$ ), closely followed by SWC in 2017 ( $r_s = -0.32$ ) and 2018 ( $r_s = 0.23$ ) with no correlation in 2019. Air temperature demonstrated a positive partial correlation in all three years ( $r_s = 0.16-0.33$ ).

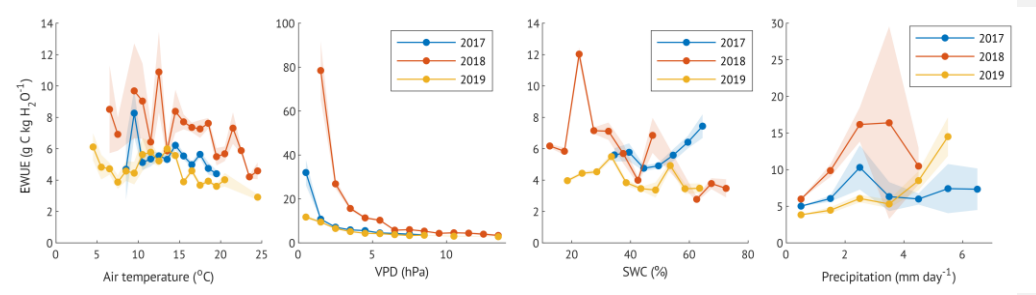


Figure 7: The impact of air temperature (a), vapour pressure deficit (b), soil water content (c) and precipitation on EWUE. EWUE was calculated as the ratio of bin-averaged daily GPP to bin-averaged daily ET, based on the averages of 1-degree Tair bins, 1hPa VPD bins, 5% SWC bins, 1mm precipitation bins with the minimum of three days per bin. The bin size was chosen based on the data availability. Shaded area denotes standard error.

#### 670 4. Discussion

675

685

690

665

While our study covered only three years, the contrasting environmental conditions provided a unique opportunity to assess *C* and water exchange under distinct moisture regimes. The study years ranged from a wet year (2017) to a drought year (2018) and an intermediate year (2019) in terms of SWC and air temperatures, additionally allowing for an assessment of potential short term legacy effects. Despite pronounced differences in meteorological conditions, the site remained a strong net *C* sink throughout the study period, with annual NEE ranging from 496 to 663 g C m<sup>-2</sup> y<sup>-1</sup>. Notably, the warmest and driest year, 2018, exhibited the highest net *C* uptake, a pattern driven by enhanced GPP in spring and suppressed ER in late summer and autumn months.

Interannual differences in water fluxes were more pronounced. ET was the lowest in 2018, leading to a markedly higher EWUE, which increased by 40% relative to the average of the other two years. The reduction in ET, coinciding with elevated VPD, suggests that stomatal regulation constrained water loss under drier conditions. Seasonal patterns further revealed a midsummer decline in canopy photosynthetic capacity (GPP<sub>sat</sub>) in all years, with the most pronounced reduction occurring in 2018 when SWC was at its lowest.

Taken together, these results indicate that the grey alder forest maintained high C uptake efficiency under hot and dry conditions, likely due to the combined effects of reduced respiratory losses and optimized water use. However, the enhanced midsummer depression in GPP<sub>sat</sub> suggests that photosynthetic activity was nonetheless constrained during peak drought periods, highlighting physiological trade offs under moisture limited conditions. These findings highlight the capacity of riparian grey alder forests to function as persistent C sinks even under variable climate conditions, yet also underscore the importance of evaluating their long term resilience under increasingly frequent climate extremes.

#### 4.1 Carbon balance

#### 4.1 Alder forest as a strong net carbon sink

Alder is a widely distributed tree species across hemiboreal and temperate zones, commonly found in riparian buffers, yet data on itsalder forest Cecosystem carbon exchange remain surprisingly searcelimited. In a chronosequence of alder forest stands, in Estonia studied by Uri et al. (2017), the two oldest forest ("Kalliste") was sites ("Agali" and "Kolleste 2") were of similar

age as (~35 and ~40 years old, respectively) to the current siteone at the time of the research (40 years old). The total annual net ecosystem-measurement. Uri et al. (2017) applied a biometric methodology, which integrates stand biomass, production (NEP) of Kalliste stand was ~77 g C m<sup>-2</sup> y<sup>-1</sup> denoting the site as a weak net C source ecosystem (NEP = NEE, Chapin et al., 2011), while the average of ~586 g C m<sup>-2</sup> y<sup>-1</sup> makes our site a strong sink of C. The differences in C balance between the sites likely stem from differences in, litterfall, and monthly soil fertility, as the Kalliste stand was established on former grassland, whereas the present site is located on nutrient rich former agricultural land. These findings highlight the role of soil fertility in determining forest C sequestration potential.

695

700

705

715

720

Compared to previously reported values for broadleaved forests in boreal and hemiboreal zones, the NEE at our site exceeds most estimates but aligns with fluxes observed in more southern broadleaved and coniferous forests (Table 3). While GPP at our site was comparable to that of boreal and hemiboreal forests, ER was notably lower. In contrast, forests with a similar NEE range (for example, in southern Sweden, Denmark, and Germany) exhibited higher GPP but also greater ER, likely driven by their warmer and sunnier climate. Riparian forests, such as our study site, receive substantial inputs of leaf litter and organic material, yet decomposition rates can be constrained by wet soil conditions. In waterlogged or anoxic layers, organic matter breaks down more slowly, potentially contributing to lower ER. Additionally, alder forests are known for their rapid growth and high nitrogen cycling (Aosaar et al., 2012; Rytter and Rytter, 2016; Uri et al., 2017), which may enhance GPP without necessarily accelerating decomposition if soil moisture remains high. On the other hand, reduced soil water availability during the drought year appeared to suppress heterotrophic respiration while GPP remained mostly unaffected. Rapid fluctuations in SWC, that are characteristic for riparian ecosystems, could potentially dampen decomposition rates, leading to lower annual ER.

Table 3. Comparative table of net ecosystem exchange (NEE), gross primary production (GPP) and ecosystem measurements to estimate carbon exchange components. Although this approach differs from the eddy-covariance method used here and the results are not directly comparable, it is possible to approximate NEE, GPP, and ER from their data under a set of assumptions (see Appendix D for details). The calculated values of NEE, GPP, ER, and total soil respiration (ER) from various broadleaf forests and forests with values close to this study. All numbers are in g C m<sup>-2</sup> y<sup>+</sup>Rs) from Uri et al. (2017), averaged over two years for Agali and based on one year for Kolleste 2, are summarised in Table 2 together with the sites' characteristics.

Table 2. Site characteristics and carbon exchange parameters from the current study and from two mature alder forests reported in the chronosequence study by Uri et al. (2017). NEE, GPP, and ER for "Agali" and "Kolleste 2" were calculated using Rs data from Table 8 and Rh, NEP, and NPP data from Table 9 in that study, following the method described in the Appendix D.

Site	Age Soil type	Bulk dens	ity pH <sub>KC</sub>	som	C:N	NEE	GPP	ER	Reference
descripti	0	g cm <sup>-3</sup>		<u>%</u>		g C m <sup>-2</sup> y <sup>-1</sup>	g C m <sup>-2</sup> y <sup>-1</sup>	g C m <sup>-2</sup> y <sup>-1</sup>	Rs
n									g C m <sup>-2</sup> y <sup>-1</sup>
Mature	~40 <u>Gleyic</u>	1.70	5.3	6.5	11.5	$-586 \pm 85$	$-1330 \pm 82$	$743\pm166$	This study-
alder fore	est <u>Luvisol</u>								
<del>in</del>									
Estonia Th	is								
<u>study</u>									
Mixed	- <del>80</del> - <u>Umbric</u>	- <u>1.00</u>	(Blac	± 7.5	11.9	<u>-386 ± 40</u>	-1537 ± 141	1151 ± 102	<u>590 ± 85</u>
broadleaf	Planosol		et a	<del>1.,</del>					
forest	<del>in290</del> ∼		2000	<u>)5</u>					
boreal	<u>35</u>		<u>.9</u>						
Canada <sub>Ag</sub>	al								
i									

Inserted Cells
Inserted Cells

Inserted Cells	
Inserted Cells	
Inserted Cells	
Inserted Cells	

Kolleste 2	<u>~40</u> <u>Gleyic</u>	0.93	3.7	<u>7.2</u>	13.3	<u>77</u>	<u>-1170</u>	<u>1246</u>	<u>990</u>	
	<u>Podzol</u>									

While our site acted as a strong net carbon sink, the two sites from Uri et al. (2017) were a much weaker sink (Agali) and a net carbon source (Kolleste 2). The GPP of our site was intermediate between the two, yet ecosystem respiration was 1.5 to 1.7 times lower. These differences can partly stem from contrasting soil properties: the current site's Gleyic Luvisol exhibited much higher bulk density (1.7 g cm<sup>-3</sup>), moderate acidity (pH 5.3), and lower soil organic matter content (6.5%) compared to the other sites, which had lighter soils, higher SOM, and, in the case of Kolleste 2, strongly acidic conditions (pH 3.7). Higher bulk density likely limits soil aeration and microbial activity, reducing respiration rates and favouring net carbon uptake, while more acidic soils and higher organic matter at Kolleste 2 may promote microbial respiration, resulting in enhanced soil respiration and, consequently, net carbon release. However, it should be noted that the study periods differ; Uri et al. (2017) conducted measurements between 2011 and 2014, whereas the current study covers 2017 to 2019, and interannual weather variability during these periods may have contributed to observed differences in carbon fluxes.

730

740

In the same years of measurement, a mature upland pine forest growing on sandy soil in Estonia exhibited similar GPP but higher ER, resulting in a weaker net carbon sink (Table 3). Compared to previously reported values for various broadleaved forests in boreal and hemiboreal zones, the NEE at our site exceeds most estimates but aligns with fluxes observed in more southern broadleaved and coniferous forests. While GPP at our site was comparable to that of boreal and hemiboreal forests, ER was, again, notably lower. In contrast, forests with a similar NEE range exhibited higher GPP but also greater ER, likely driven by their warmer climate with a longer active vegetation season.

Very low ER in our study likely reflects oxygen limitation in a compact, frequently wet mineral soil, rather than nutrient shortage. The slightly acidic soil with high bulk density forms conditions that reduce gas diffusion and favour anoxic microsites, suppressing microbial decomposition despite moderate total C. Together with restricted fine-root activity under dense, saturated conditions, these factors could lead to low ecosystem respiration. We note, however, that our observations are limited to three years with exceptional weather conditions, which may not fully capture the "typical" respiration rates of this forest

Table 3. Net ecosystem exchange (NEE), gross primary production (GPP), and ecosystem respiration (ER) reported for broadleaf forests and sites with values comparable to this study. "(s. yrs.)" indicates that averages were calculated using only the same years as in this study (2017–2019). All values are in g C m<sup>-2</sup> y<sup>-1</sup>, mean ± SD where available.

Site description	NEE	<u>GPP</u>	ER	Reference
	g C m <sup>-2</sup> y <sup>-1</sup>	g C m <sup>-2</sup> y <sup>-1</sup>	g C m <sup>-2</sup> y <sup>-1</sup>	
Mature alder forest in Estonia (2017-2019)	<u>-586 ± 85</u>	<u>-1330 ± 82</u>	<u>743 ± 166</u>	This study
Pine forest in Estonia (s. yrs.)	<u>-214 ± 113</u>	$-1264 \pm 49$	$\underline{1050\pm118}$	(Rogozin et al., in print)
Beech forest in Denmark (s. yrs.)	<u>-282 ± 51</u>	-2072 ± 122	$1849 \pm 169$	(Pilegaard and Ibrom, 2020)
Oak forest in boreal Canada	-206 ± 92	-1343 ± 85	1171 ± 139	(Beamesderfer et al., 2020)
Alder/Ash mixed forest in Germany	-193	-1595	1401	(Kutsch et al., 2005)
Beech forest in Denmark	<del>-313.6353.8</del>	<del>-1977.42302.4</del>	<del>1663.8 1948.6</del>	(Lindroth et al., 2020)
Oak-dominated forest in Germany	-559	-1794	1235	(Kutsch et al., 2005)
Mixed deciduous forest in Germany (s. yrs.)	<u>-372 ± 91</u>	-1497 ± 181	<u>1117 ± 91</u>	(Pohl et al., 2023)

Spruce forest in Germany	<del>-663 ± 78</del> <del>or-</del> -535 ± 72-*	<del>-1680 ± 103</del> <del>or</del> -1755 ± 249-*	1020 ± 106 or-1219 ± 232-*	(Ney et al., 2019)
Beech forest in France	- <u>386</u> ± 171	-1347 <u>±</u> ± 192	$1011\pm138$	(Granier et al., 2008)
Spruce forest in Southern	<del>-192.9582.3</del>	<del>1851.6 1869.0</del>	<del>1286.81658.7</del>	(Lindroth et al., 2020)
Sweden				
Pine forest in  EstoniaRiparian poplar plantation in China (growing season values)	$-214 \pm 113928 \pm 141$	<del>-1264 ± 491984 ±</del> 191	$\frac{1050 \pm 118}{1056 \pm 55}$	(RogozinXu et al., in print2020b)

<sup>\*</sup>depending on the gas analyser heating correction

#### 4.2 Water exchange and water use efficiency

Distinct seasonal patterns in ET in our study were shaped by the interplay of key environmental factors, including Rg, VPD, air temperature and precipitation (Brümmer et al., 2012; Jassal et al., 2009; Massmann et al., 2019). The close alignment between the seasonal cycles of ET and GPP further supports the long established coupling of plant water and C exchange through stomatal regulation (Jarvis, 1986). The mid-season decline in ET, which coincided with a similar reduction in GPP, was likely a response to lower VPD and diminished solar radiation—both identified as primary regulators of ET (Jassal et al., 2009). This decline was particularly pronounced in 2018, when prolonged drought conditions and limited precipitation further constrained ET. The bell-shaped response of ET to SWC resulted in reduced total water fluxes in growing seasons with both high (2017) and low (2018) SWC, whereas total ET peaked in 2019 under intermediate soil moisture conditions. These findings underscore the dual influence of atmospheric and soil moisture controls on ET dynamics and high light the sensitivity of alder forest water fluxes to interannual variability in hydroclimatic conditions.

The evapotranspiration to precipitation ratio (ET/P) provides further insight into the site's water balance and its response to changing hydroclimatic conditions. During the May September of 2017 (the "wet" year), ET nearly equalled precipitation (ET/P = 0.98), suggesting that the most of precipitation was used for transpiration and soil and wet surface evaporation, with minimal excess contributing to runoff or deep percolation. In contrast, the same months of 2018 (the drought year) exhibited the lowest ET/P ratio (0.76), indicating a precipitation surplus and constrained water loss, likely due to stomatal closure in response to soil moisture depletion and high VPD. The ET/P ratio increased again in 2019 (ET/P = 0.83, in May September), suggesting a partial recovery in transpiration as soil moisture availability improved. This interannual variability highlights the forest's capacity to adjust water use under different climatic conditions, with a clear suppression of ET during drought and a subsequent increase as conditions became more favourable.

The EWUE in our study was notably higher than reported for various forest ecosystems globally. The average EWUE of 5.3 ± 1.2 g C kg H<sub>2</sub>O<sup>-1</sup> exceeded values observed in mixed temperate forests (1.9–4.1 g C kg H<sub>2</sub>O<sup>-1</sup>; Jin et al., 2023), deciduous forests in the USA (2.3–2.7 g C kg H<sub>2</sub>O<sup>-1</sup>; Xie et al., 2016) and Central China (2.6 ± 0.7 g C kg H<sub>2</sub>O<sup>-1</sup>; Niu and Liu, 2021), as well as the global range for forested ecosystems (0.8–3.6 g C kg H<sub>2</sub>O<sup>-1</sup>; Zhou et al., 2014), suggesting that high EWUE may be a characteristic feature of nitrogen-fixing riparian forests. The ability of the alder forest to maintain elevated EWUE, suggests an efficient water conservation strategy that supports sustained C assimilation under varying moisture conditions.

775 This trait may

765

Anoxic conditions, combined with fluctuating soil moisture levels, are very favourable for methane (CH<sub>4</sub>) production (Dlugokencky et al., 2011; Feng et al., 2020; Flanagan et al., 2021). In addition, the high N content typical of alder forests could promote nitrous oxide (N<sub>2</sub>O) emissions (Butterbach-Bahl et al., 2013; Davidson et al., 2000). In principle, these non-CO<sub>2</sub> fluxes could offset the strong net carbon sink observed in our study. However, chamber-based and eddy-covariance measurements at the site (Mander et al., 2021, 2022) indicate otherwise. On an annual scale, the alder stand functioned as a

very minor CH<sub>4</sub> sink, contributing merely 0.1% to the total GHG global warming potential (Table E1). While annual N<sub>2</sub>O fluxes were positive, they represented just 1.1% of total NEE in CO<sub>2</sub>-equivalent units (or 7.9% based on chamber-derived estimates), too small to negate the forest's role as a substantial net CO<sub>2</sub> sink.

#### 4.2 Lower than expected evapotranspiration

785 Evapotranspiration (ET) integrates physical evaporation from soil and wet surfaces with plant transpiration, making it inherently complex (Brümmer et al., 2012; Jarvis, 1986; Jassal et al., 2009; Massmann et al., 2019) and difficult to quantify accurately (Fisher et al., 2017). Eddy covariance estimates are further affected by incomplete energy balance closure (Appendix A) (Amiro, 2009; Foken, 2008; Mauder et al., 2018, 2020). We chose to report the ET based on directly measured LE, as net radiation and ground heat flux were not available for accurate adjustment (Mauder et al., 2018)

Annual ET in the wet year 2017 (255 mm y<sup>-1</sup>) and especially in the drought year 2018 (194 mm y<sup>-1</sup>) were lower than expected for the boreal and hemiboreal region (Launiainen et al., 2022; Lindroth et al., 2020; Wang et al., 2021) and much lower than in the various riparian forests (Kochendorfer et al., 2011; Kowalska et al., 2020; Scott et al., 2004; Xu et al., 2020b). However, ET in the recovery year 2019 (342 mm y<sup>-1</sup>) was much closer to previously reported annual ET values in boreal and hemiboreal forests in 2015-2018 (Lindroth et al., 2020) and multi-year averages reported by Wang et al. (2021) (384 ± 12 mm y<sup>-1</sup>) and Launiainen et al. (2022) (348 ± 26 mm y<sup>-1</sup>). The average precipitation during the growing season in the latter study (383 ± 83 mm) was comparable to our wet (372 mm) and recovery (338 mm) years but exceeded the drought year (271 mm), indicating that lower atmospheric water supply likely contributed to the reduced ET in 2018. Lower ET under higher precipitation in the wet year may be explained by cooler summer temperatures reducing evaporative demand. On the other hand, lower energy balance closure levels in 2017 and 2018 (70% and 71%, respectively) might contribute to the ET underestimation (Figure A1).

Furthermore, the low ET with sufficient GPP results in notably higher annual EWUE (5.3 ± 1.2 g C kg H<sub>2</sub>O<sup>-1</sup>), which exceeded values (0.9 – 4.1 g C kg H<sub>2</sub>O<sup>-1</sup>), previously reported for various forests (Jin et al., 2023; Niu and Liu, 2021; Xie et al., 2016; Zhou et al., 2014).

The evaporative index (ET/P) in 2017 and 2018 (0.69 and 0.67, respectively) was consistent with values reported for other forested ecosystems (Williams et al., 2012), whereas a higher ratio of 0.92 in 2019 likely reflects the combined effects of a warm growing season and well-distributed precipitation, which stimulated both photosynthesis (Table 1) and transpiration (Figure 9). As previously demonstrated by Eschenbach and Kappen (1999), alder's high leaf stomatal conductance supports enhanced transpiration under adequate water supply, implying that conditions in 2019 may have been near optimal for maximising water and carbon exchange. We have to note that the evaporative index remained below one in all years of our study, which is surprising for a riparian forest that typically has access to additional water through lateral inputs, and thus ET would exceed P (Kochendorfer et al., 2011; Xu et al., 2020b). The shallow and narrow forest river near our study site likely provided only limited supplemental water. While this forest is experiencing seasonal flooding, it might be a result of historically formed high-density soils, rather than the river's impact in the three studied years.

## 4.3 Moderate soil saturation enhances ecosystem fluxes

815

820

Soil moisture variability plays an important role in modulating ecosystem carbon exchange, although its effect is usually more pronounced in water-limited, rather than radiation-limited regions (Green et al., 2019; Kannenberg et al., 2024). Nevertheless, variable soil moisture conditions are intrinsic to riparian forests, where seasonal flooding and fluctuating groundwater table create a dynamic hydrological regime (Kowalska et al., 2020; Portela et al., 2023; Singer et al., 2014). On our site, the variation in soil saturation (SSR) levels caused a non-linear response of canopy gas exchange, with both very dry and very wet conditions constraining reference stomatal conductance (Gc<sub>ref.</sub> Gc at 1kPa of VPD, "the maximum stomata aperture") (Figure 6). Soil moisture extremes impose both hydraulic and metabolic constraints: low saturation limits water supply to leaves, while high saturation can cause oxygen limitation in the rhizosphere, impairing root function and nutrient uptake (Kochendorfer et al.,

2011; Kozlowski, 1997). The physiological optimum for canopy conductance at a moderate soil saturation (~40–50%) was reflected in photosynthetic capacity and transpiration and enhanced carbon and water fluxes in the corresponding growing season periods of different years.

Relatively high values of photosynthetic capacity and ET, sustained into wetter ranges during summer months, especially during the colder year, may reflect adaptations to periodic flooding typical of riparian forests. Canopy EWUE declined with increasing soil water content in the wet year, consistent with a "relaxed" physiological state when water is not limiting.

Reference respiration (ER<sub>ref</sub>) also followed a similar saturation curve, with moderate soil moisture promoting optimal metabolic activity, while substrate constraints under lower saturation ratios reduced respiration rates.

#### 830 4.4 Alder forest in the 2018 drought year

840

845

850

In 2018, low precipitation caused widespread soil moisture deficits across Europe, while extremely high air temperatures further intensified drought conditions through elevated VPD (Fu et al., 2020; Lindroth et al., 2020; Smith et al., 2020). Estonia also experienced two extended dry spells (in May and July), accompanied by an exceptional heat anomaly from mid-July to early August (Krasnova et al., 2022). These conditions produced a progressive summer drought at our site (Figure 7).

In May, while the soil drying was faster than in July, it reached only ~50% soil saturation, which persisted through June. We found this moisture level to be optimum for ecosystem fluxes (Figure 5) and plant stomatal activity (Figure 6), although still constrained by the early stages of the growing season. The relatively low canopy conductance at that time likely reflected ongoing alder leaf development. Under these favourable early-season water conditions and warmer-than-average May temperatures, all fluxes and canopy physiological parameters gradually increased (Figure 7).

Higher spring temperatures can enhance the ecosystem's resilience to future climatic extremes, reinforcing the potential role of grey alder forests in maintaining regional C sinks under shifting hydroclimatic regimes.

## 4.3 Drought impact and the absence of legacy effect

Despite the 2018 heatwave, the grey alder forest remained a strong C sink, exhibiting the highest net C uptake of the study period. In spring, increased GPP drove a higher net uptake, while in late summer and autumn, suppressed ER was the primary contributor to enhanced NEE. Warmer spring temperatures have previously been shown to stimulate net Cannual net carbon uptake by extending the growing season (Keenan et al., 2014; Wolf et al., 2013) as was also observed in our study, and offsetting the influence of the forthcoming summer drought on the annual Ccarbon balance (Angert et al., 2005; Kljun et al., 2006; Smith et al., 2020; Wolf et al., 2016). A similar pattern was reported for a floodplainriparian mixed broadleaf forest in the Czech Republic, where an anomalously warm spring in 2018 led to an increase in both GPP and ET, counteracting the negative effects of the summer drought (Kowalska et al., 2020). In boreal and hemiboreal regions, moderate spring warming in spring typically coincides with sufficientample soil moisture availability from snowmelt, ensuring adequatesufficient water supply for early-season C assimilation. However, enhanced spring productivity and transpiration can also accelerate soil water depletion, increasing susceptibility to summer drought stress (Bastos et al., 2020).

The impact of 2018 drought on various Nordic forests was analysed by Lindroth et al. (2020). In a beech forest, the only broadleaved forest included in their analysis, both GPP and ER decreased by approximately 300 g C m<sup>-2</sup> y<sup>-1</sup>, with GPP experiencing a slightly stronger reduction, leading to a minor decrease in annual NEE. In contrast, the forest in our study exhibited a much smaller annual change in C fluxes, with GPP and ER declining by only 52.5 and 116.2 g C m<sup>-2</sup> y<sup>-1</sup>, respectively. The stronger suppression of ER compared to GPP was likely the key factor maintaining high net C uptake in 2018.

860 Water fluxes were more strongly affected by the drought. ET was significantly reduced (for 35%) in 2018, leading to the highest EWUE of the three study years (40% higher than the average of the other two years). EWUE is often used as an indicator of a forest's ability to optimize C assimilation under changing water availability (Huang et al., 2015; Keenan et al.,

2013; YangIn July 2018, the soil moisture decreased further, reaching a minimum by August. Combined with extremely high temperatures and VPD peaks, the progressive drought suppressed all gas fluxes and vegetation activity (Figure 7). The drought resistance indices, calculated for May-September, indicated average reductions of 15%, 37%, and 43% in daily GPP, ET, and ER, respectively, relative to 2017 (Figure 9). The reduction of GPP in summer 2018 is in line with observations from multiple sites across Europe (Fu et al., 2020; Lindroth et al., 2020) and can be attributed to stomatal regulation under the lack of soil water availability. Indeed, we estimated a 61% decline in daily Ge over May-September 2018. After the initial increase in May-June, it continuously declined through July and remained low until the end of the growing season (Figure 4d, Figure 7). 870 This explains the suppressed canopy photosynthetic capacity in August 2018, especially when compared to the peaking values in the reference year (Figure 4b).

865

880

885

The Gc suppression was likely driven by high atmospheric demand (i.e. increasing VPD) rather than soil moisture depletion, as indicated by uniformly low values of Gcref across all SSR classes in the active season of 2018. High VPD can override soil moisture gradients, forcing sustained stomatal downregulation regardless of soil moisture variation (Novick et al., 2016).

Maintaining or increasing EWUE during unfavourable or extreme conditions provides the ecosystem with a sufficient reserve of carbohydrates, which may later facilitate recovery. Conversely, less flexible ecosystems may experience C deficiency that eould also be reflected in subsequent years (Frank The reduction of stomatal conductance to prevent water loss has been previously documented across multiple plant species and forest types (Farquhar and Sharkey, 1982; Fu et al., 2020; Lindroth et al., 2015; Kannenberg 2020; van der Molen et al., 2020). An increase in 2011; Novick et al., 2016; Reichstein et al., 2002), reflecting a conservative hydraulic strategy of our study site.

Since both GPP and ET are mechanistically connected with stomatal regulation, the low ET resistance is not surprising; however, its sensitivity was much higher than that of GPP (37% decline compared to only -15%). Total ET includes both transpiration (T) and evaporation, though the latter is limited under drought. However, even when filtering only for the periods with maximum T contribution, the drop in daily values (-29%) still exceeded that of GPP (Figure 9). This additionally contradicts the findings of Lindroth et al. (2020), where the majority of sites demonstrated an increase in ET in the drought year. Boese et al. (2019) found that the sites with high seasonal dryness variability experienced a lower ET decrease rate during the progressive drought due to plant adaptations such as deeper root systems to access the water. However, at our site, high soil moisture variability is skewed towards flooding rather than drying, which is consistent with the sharp drop in ET over the course of the July progressive drought (Figure 2, Figure 3).

The greater ET sensitivity compared to GPP resulted in enhanced daily EWUE (+38%, Figure 9) over May-September. An elevated EWUE during drought, as observed in our study, has been previously reported, for example, for a boreal aspen stand in Canada (Krishnan et al., 2006) and a mixed deciduous forest in SwitzelandSwitzerland (Wolf et al., 2013). However, responses appear to be species- and site-dependent; for example, no change in EWUE was observed in a Finnish forest under low rainfall conditions (Ge et al., 2014), while a decline in EWUE was reported for a pine forest in Finland under severe drought stress (Gao et al., 2017). These contrasting patterns highlight the importance of species-specific drought adaptation

strategies and site hydrology in determining forest water use responses.

The midseason reduction in canopy photosynthetic capacity (GPP<sub>sea</sub>) under high temperatures and low soil moisture suggests physiological constraints on photosynthesis under limiting conditions. A similar, though less pronounced, reduction was observed in 2019, pointing to a potential legacy effect. However, total GPP in 2019 was the highest of the study period, and the concurrent increase in ET led to a lower EWUE. Combined with higher ER, these findings suggest that the ecosystem was in a recovery phase rather than experiencing prolonged drought-induced C limitations. Moreover, the difference between GPPsat of all three studied years was not significant, denoting alder forest under study as a functionally stable ecosystem (Chen

Although daily EWUE declined during progressive drought in July, VPD-normalised EWUE remained elevated throughout the drought, indicating that high atmospheric demand combined with soil moisture limitation drove the observed water use

efficiency dynamics. Similar increases in VPD-normalised EWUE under moderate drought have been reported across forest and grassland ecosystems (Beer et al., 2009).

Interestingly, ER resistance was nearly twice as low as that of GPP (Figure 9), pointing to a strong drought impact on soil microbial and root respiration. This reduction in ER effectively lengthened the period of ecosystem net carbon uptake and, combined with the favourable early-season conditions in May, resulted in the highest annual net carbon uptake of the three study years.

#### 4.5 Drought recovery and carry-over effects

935

Drought can influence ecosystem functioning well beyond the event itself, with lagged effects persisting for years after water stress has ended (Kannenberg et al., 2020). In forests, such "drought legacy effects" are common and often span three to four years (Anderegg et al., 2015). They could be caused by the carbon depletion due to reduced uptake during the drought (Bréda et al., 2006; McDowell et al., 2008), the cost of repairing hydraulic damage (Anderegg et al., 2015; Kannenberg et al., 2019), changes in the nutrient cycle (Houle et al., 2016; Schlesinger et al., 2016), or from shifts in carbon allocation towards root development or canopy restoration (Arain et al., 2022; Doughty et al., 2014; Hikino et al., 2022), all of which can constrain subsequent tree growth and ecosystem functioning.

920 Although our study period was too short to assess long-term drought legacies, it allowed us to evaluate recovery and possible carry-over effects in the year following the 2018 drought. In 2019, GPP, ER, and ET reached their highest values of the three study years, both annually and during the active season (Table 1). Recovery indices indicated full recovery of all fluxes, with daily active-season ET and T even exceeding that of the reference year (Figure 9).

While soil moisture was declining over the recovery year summer, the evenly distributed precipitation kept the favourable soil
saturation rates over all months, contributing to the ecosystem recovery (Figure 2). Soil water depletion in riparian systems
can vary considerably depending on groundwater connectivity, precipitation patterns, and vegetation water use (Capon et al.,
2013). In systems with strong hydrological connectivity to groundwater, depletion may be minor; however, under drought
conditions or in systems with limited lateral or vertical recharge, significant drawdown can occur (Rohde et al., 2021; Rood et
al., 2008). At our site, in the absence of runoff or drainage measurements, we cannot fully quantify the water balance, and our
interpretation of groundwater connectivity remains speculative.

The nearly 30% increase in annual ER in 2019 relative to the pre-drought year, and 55% relative to 2018, likely reflected a combination of higher spring temperatures in the recovery year and a pronounced June–July peak in ER<sub>ref.</sub> that cannot be explained by temperature alone (Figure 4a). This interpretation is supported by the absence of differences in active-season daily ER between 2017 and 2019 when modelled using each other's temperature response parameters (Figure 8d-e). Similarly, although the recovery index of ER<sub>ref.</sub> was slightly lower than that of ER during the active season, neither differed significantly from each other or from 1, indicating full recovery (Figure 9). An increase in ecosystem respiration in the year following the drought was also observed in a beech forest in Denmark (Pilegaard and Ibrom, 2020), attributed to accumulated soil organic matter following suppressed heterotrophic respiration during the drought and autumn months, and for a ponderosa pine forest in the USA (Thomas et al., 2009), where the effect was linked to enhanced litter decomposition.

940 Likewise, the increase in GPP, though less pronounced than in ER, was caused by a combination of vegetation activity and meteorological conditions. In 2019, elevated temperatures and higher radiation compared to 2017 advanced the onset of the growing season. Enhanced GPP<sub>sat</sub> suggests that optimal temperature and VPD, rather than light, were the main drivers at that stage. Later in the season, GPP<sub>sat</sub> was lower than in 2017, yet modelled values converged, particularly in August (Figure 8a), pointing to lower radiation as the primary carbon uptake constraint. As with ER, both GPP<sub>sat</sub> and GPP demonstrated full 945 recovery (Figure 9).

While transpiration and photosynthesis recovered fully, stomatal conductance recovery was incomplete (Rc = 0.87), and resilience was reduced (Rs = 0.79), indicating that subtle physiological constraints persisted despite overall functional

recovery, potentially limiting tolerance to future droughts. However, as these indices are based on a single pre-drought reference year, interannual variability in meteorological conditions may bias interpretation. Favourable conditions in 2019, including evenly distributed precipitation and a warm growing season, likely facilitated the rapid recovery, consistent with observations across diverse ecosystems (Schwalm et al., 2017).

In contrast, strong legacy effects on the <u>Gearbon</u> cycle have been observed following the 2018 drought in other European forests. For example, in a mixed deciduous forest in central Germany, NEP declined by 150 g C m<sup>-2</sup> y<sup>-1</sup> in 2019, with reductions in both GPP (-281 g C m<sup>-2</sup> y<sup>-1</sup>) and ER (-132 g C m<sup>-2</sup> y<sup>-1</sup>) compared to the previous year (Pohl et al., 2023). European beech forests have exhibited particularly high sensitivity to drought, with observed tree mortality linked to hydraulic failure (Rukh et al., 2023; Schuldt et al., 2020). More broadly, drought-induced tree mortality can have long-lasting consequences, with post-drought effects often persisting for months or years (Brodribb et al., 2020; Schwalm et al., 2017). A global synthesis showed that drought legacy effects are widespread in forests, typically lasting three to four years (Anderegg et al., 2015), with post-drought temperature and precipitation conditions strongly influencing recovery time (Schwalm et al., 2017). Drought-related growth decline and canopy dieback have also been documented in various riparian trees (Kibler et al., 2021; Schnabel et al., 2022; Singer et al., 2013; Stella et al., 2013; Valor et al., 2020). In our study, we foundOur site provided no visual or statisticalnumerical evidence of increased tree mortality in the year following the 2018 drought. However, given that drought-induced mortality can manifest with a delay, it remains possible that long-term effects could emerge beyond the period of our study. Future monitoring would be critical to assessing whether the observed recovery is sustained or whether cumulative drought stress could compromise forest resilience over time.

#### 4.4 Sustainability and forest management considerations

The benefits of grey alder in forestry are well recognized across the Nordic and Baltic regions, where it is valued for its rapid early growth, high productivity, nitrogen-fixing capacity, broad ecological range, frost resilience, and relatively low susceptibility to pests. The recommended harvesting age for grey alder stands is typically between 20 and 25 years (Uri et al., 2014), although significant increases in woody biomass continue beyond this age. For instance, Aosaar et al. (2012) suggested that the optimal age for harvesting could be closer to 40 years. Our findings demonstrate that even at this advanced age, the riparian grey alder forest remained a strong C sink, showing no clear evidence of a drought legacy effect following the 2018 heatwave. However, as drought induced mortality can occur with a delay, a single post drought year may be insufficient to assess potential long-term resilience. While the forest is considered ready for harvesting, the trade-off between maximizing short-term timber revenue and sustaining long-term C sequestration remains uncertain. These considerations highlight the need for longer-term research, particularly on the C balance and drought resilience of riparian alder forests beyond 40 years of age, to guide both sustainable management strategies and climate mitigation efforts.

## 5. Conclusions

950

955

970

975

The mature riparian grey alder forest <u>under study</u> remained a strong and consistent net <u>Ccarbon</u> sink <u>aerossover</u> three years with contrasting soil moisture conditions. The <u>highest net C uptake in 2018</u>, <u>despite the heatwave and drought</u>, <u>While GPP</u> was driven primarily by suppressed comparable to that of similar ecosystems, ER in response to moisture limitation, with only a <u>minor impact on GPP</u>. <u>Similarly</u>, ET was <u>significantly generally lower</u>, <u>likely due to dense</u>, <u>poorly aerated soils and periodic flooding</u>.

Moderate soil saturation ratio (40–50%) enhanced ecosystem fluxes, with flux rates generally persisting even at higher saturation levels. In contrast, the 2018 progressive drought mildly reduced, leading to a 40% increase in GPP and, to a much greater extent, ER, while also suppressing ET. High EWUE. While photosynthetic capacity (GPP<sub>sub</sub>) declined during the peak drought stress, there was no significant difference between the years and reduced Gc indicated stomatal regulation that minimised water loss while maintaining efficient carbon uptake. The co-occurrence of elevated temperatures (driving high

VPD) and prolonged dry spells (causing progressive drought) in 2018 proved particularly detrimental, with the canopy
 conductance suppression primarily driven by elevated VPD, while soil moisture variation played a larger role in the other two years.

In the year following the drought, the forest exhibited an overall recovery, supported by high, but not extreme, temperatures and evenly distributed precipitation. The intermediate cumulative NEE was a result of elevated ER in spring to early summer, likely due to decomposition of residual organic matter from the preceding year. GPP also increased, although to a lesser extent, with canopy conductance remaining partially suppressed, suggesting functional stability.

The absence of a clear drought legacy effect in 2019, combined with the forest's ability a potential vulnerability to sustain high EWUE and net C uptake under extreme conditions, suggests that riparian grey alder forests are highly adaptable to short-term hydroclimatic variability. Unlikemulti-year drought events.

<u>In contrast to</u> other European broadleaved forests where <u>long-lastingprolonged</u> drought impacts have been <u>observed\_documented</u>, this <u>riparian\_mature</u> alder stand maintained <u>its\_both</u> productivity and resilience. However, as drought-induced tree mortality can <u>manifestoccur</u> with a delay, <u>longercontinued long-term</u> monitoring <u>would beis</u> essential to assess whether <u>these forests remain resilientsuch resilience will persist</u> under increasing drought frequency and severity.

Balancing long term C sequestration with sustainable forest management remains a key challenge. While the forest in this study has reached a typical harvestable age, the potential trade-offs between timber production and long-term C uptake warrant further investigation. Future research should examine how stand age, site conditions, and climate extremes affect the stability of alder forests over time, as well as explore the effects of alternative management strategies, such as extended rotations or mixed-species planting, on maintaining resilience under a changing climate.

#### Appendix

995

000

005

020

## Appendix table 1. Bonferroni-adjusted p-A. Energy balance closure

To assess the performance and consistency of turbulent energy flux measurements, we evaluated the energy balance closure (EBC) on a daily timescale for June-August of each study year (2017–2019). The turbulent fluxes were defined as the sum of latent (LE) and sensible (H) heat fluxes measured using the eddy covariance system. Since the components of available energy, net radiation (Rn) and ground heat flux (G), were not measured at our site, we used the following approach.

Rn was approximated using measured incoming shortwave radiation (Rg) and daily albedo values of Wilcoxon signed rank
1015 test comparison between:

 $Rn = (1 - \alpha) \times Rg,$ 

where α is surface albedo and Rg is daily incoming shortwave radiation in MJ m<sup>-2</sup> day<sup>-1</sup>

Rg was measured at the site, and daily albedo values were derived from MODIS (MCD43A3 v061), (Schaaf and Wang, 2021) using Google Earth Engine. Extracted albedo values were averaged black-sky and white-sky shortwave albedo components to approximate actual albedo under mixed sky conditions. The data were quality-controlled using MODIS-provided QA flags and seasonally averaged, resulting in mean albedo values of 0.161±0.009, 0.154±0.007 and 0.151±0.007 in 2017, 2018 and 2019, respectively.

G was estimated as 5% of Rn, following common practice for forest soils. Only daytime (Rg >15 W m<sup>-2</sup>) half-hourly records were included in the daily energy sums to ensure that energy components reflected active turbulent exchange.

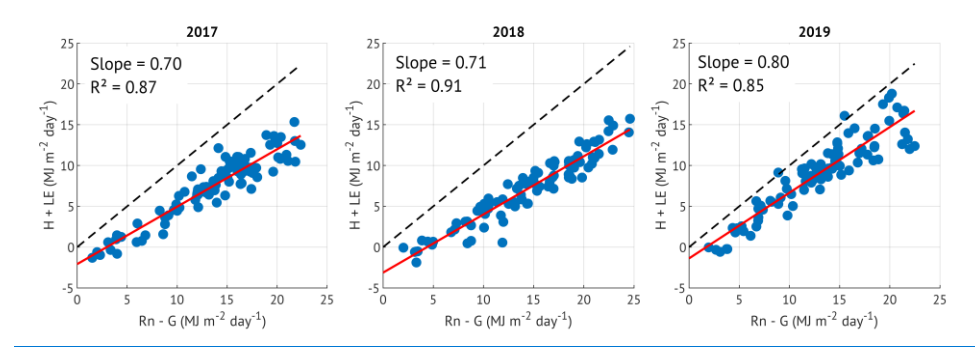


Figure A1. Energy balance closure in June-August of the three study years. Available energy is represented by net radiation (Rn) minus soil heat flux (G), turbulent energy is a sum of sensible (H) and latent heat (LE) fluxes, all aggregated over daytime periods (Rg  $\geq$  15 W m<sup>-2</sup>). The energy balance closure is expressed as the growing seasons of slope of the least squares regression, shown in red colour in each panel. The dashed lines are 1:1.

While this approach is limited by the absence of direct measurements of Rn and G, it still provides a consistent method for comparing EBC across years. Although the EBC values are on the lower end, they fall within the expected range for forested ecosystems. Moreover, the similar closure observed in 2017 and 2018 supports the interpretation that reduced evapotranspiration (ET) in the drought year (2018) was not driven by lower EBC but likely reflects actual physiological or environmental responses.

## Appendix B. Sensitivity of canopy conductance to VPD in different years. soil saturation classes

025

Table B1. Parameters of Oren et al. (1999) canopy conductance sensitivity model. The gray shading is applied to the soil saturation ratio (SSR) classes, where a low slope corresponds to the low quality of the fit

Growing seasons SSR class NEE Fixed			d slope	ERNo GP F	T EW	<del>/UE</del>	GPP
		(0.6) mod	<u>el</u>	t-fixed p slope model			capacity
		$\frac{Gc_{ref}}{(mm \ s^{-1})}$	<u>R</u> <sup>2</sup>	Gc <sub>ref</sub> (mm s <sup>-1</sup> )	<u>R</u> <sup>2</sup>	Slope	
2017 vs 2018	<u>0.1 – 0.</u> 2 <del>.42E-07</del>	2.60E-	0.220742	$4.04 \pm 0.30$	2.44E-	0.0002422	1.3101
		$\frac{164.80 \pm 0.26}{}$	<u>21</u>		<u>0.</u> 05	<u>3</u>	
201 5.60 A.67	0.0011332 - 0.3	2.25E-	1.35E-	$7.12 \pm 0.926346$	0.23	0.61	
8 vs E-07 E-19 201 9		7.11 ± 0.44	070.23				
2017 vs 2019	0.20024 1.24390	7.82 ±	0.000288	$7.82 \pm 0.0103340$	0. <del>1189</del> 0	0.23	
	63 – 0.4	0. <del>261011</del> <u>41</u>	<u>05</u>		<u>3</u>		
<u>0.4 – 0.5</u>		$     \begin{array}{r}       10.36 & \pm \\       0.47 &    \end{array} $	0.22	$\underline{10.36 \pm 0.47}$	0.22	0.54	
<u>0.5 – 0.6</u>		$\frac{8.96}{0.51}$ $\pm$	0.13	$8.86 \pm 0.51$	0.15	0.44	
0.6 – 0.7		9.15 ± 0.57	0.25	$9.09 \pm 0.57$	0.25	0.68	

Deleted Cells
Deleted Cells
Deleted Cells
Deleted Cells
Deleted Cells
Deleted Cells
Inserted Cells
Deleted Cells
Deleted Cells
Inserted Cells
Inserted Cells
Deleted Cells

0.7 - 0.8		$\underline{6.69 \pm 0.43}$	0.44	0.65
<u>≥0.8</u>	$\frac{4.65}{0.34}$ $\pm$ $0.22$	$4.59 \pm 0.35$	0.23	0.73

Appendix table 2. Spearman's coefficients (r.) from partial correlation analysis between half-hourly (ER, GPP, ET) and daily (EWUE) values and environmental drivers. Only statistically significant (p<0.05) results are presented

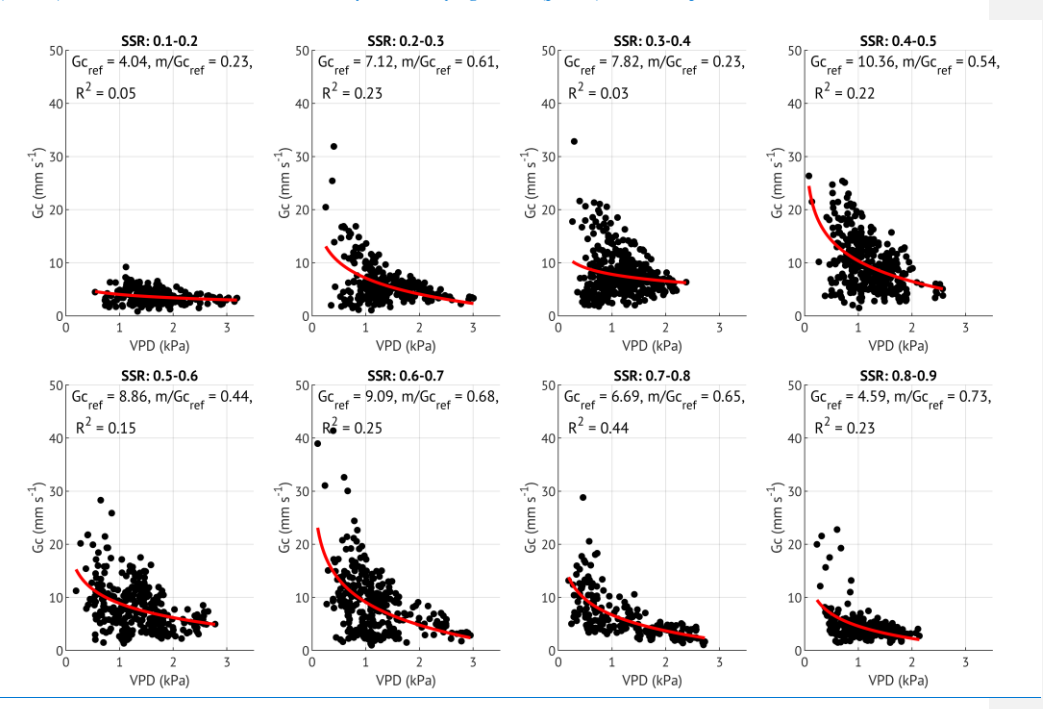


Figure B1. Oren fits with variable m to different soil saturation ratio (SSR) classes

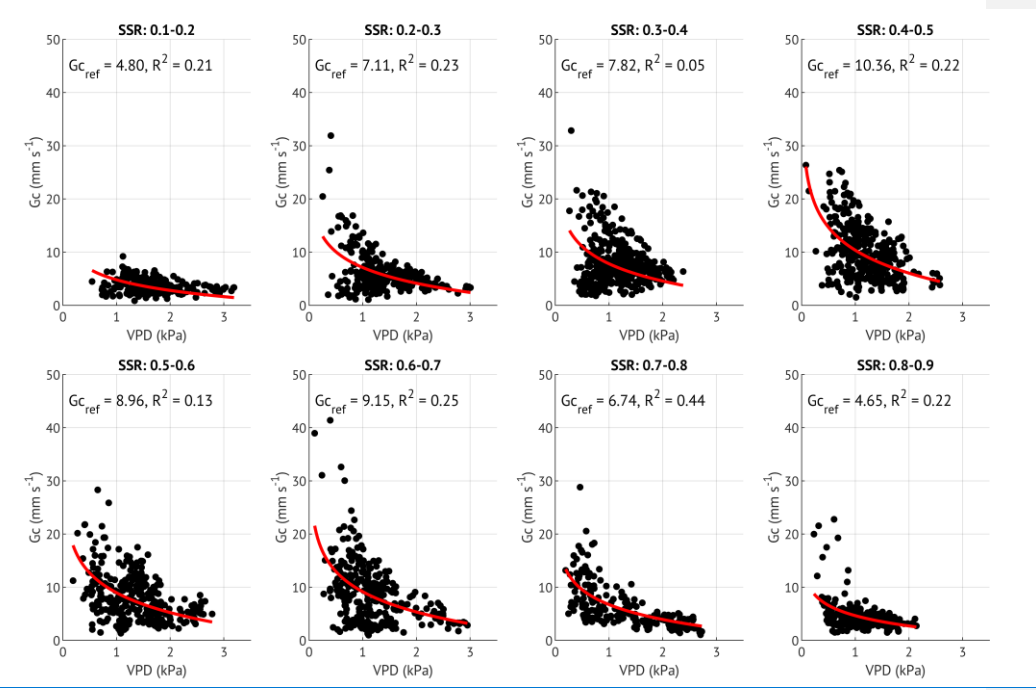


Figure B2. Oren fits with a fixed m/Gcref=0.6 to different soil saturation ratio (SSR) classes



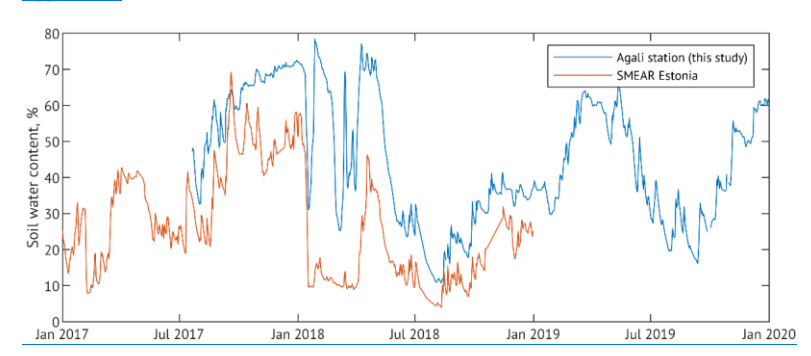


Figure C1. Soil water content at the study site (blue) and SMEAR Estonia station (red)

Table C1. Soil physical-chemical properties of the study site. Mean and standard error values (in parentheses). DM – dry matter, SOM – soil organic matter, TC – total carbon, TN – total nitrogen.

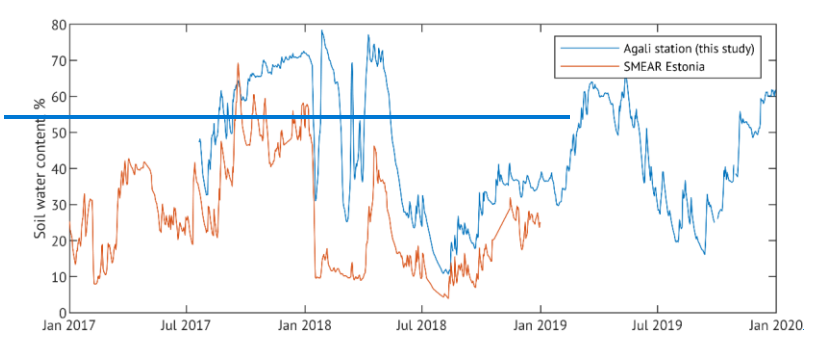
Depth cm		Night	t <del>D</del> a	<del>ıyti</del>	ETD	EWI	JE 🔏	<u>rc</u>	TN		C:N			K	<u>Ca</u>		Mg				
		ime	me	•	M	** <u>S</u>	0 0	<u>%</u>	<u>%</u>					mg	mg	kg <sup>-1</sup>	mg	kg-l			
		ER <u>Bu</u>	<u>G</u>	op <sub>p</sub>	<u>%</u>	M %	<u>ó</u>					Ī		kg-1							
		lk	$\mathbf{H}_{\mathbf{F}}$	<u>KCI</u>									ng kg								
		densi	<u>t</u>									1									
		<u>y</u>																			
		g cm	3																		
Year/driver		<del>Ts</del>	3	Rg	ŧ	VC V:		4	g	Ta		SWC	¹ <del>Ta*</del> ₽	₩ C*	45	T SWC		PD			
2 P	<del>0.</del>		- <u>5.30</u>	<u>-60</u>		6.5	- <u>3.8</u>		0.483	<u>11.</u>				5.2	0.151		).46	<u>ρ</u>	0	0	$\langle$
0 <del>.</del> 1 3		(0. <del>29</del> 0	(0.370			(0.462)	(0.5	1	3	<u>5</u>				).4 <u>59</u>	487	<u>8</u>		2	<del>.</del>	÷	
7 8	<u>0</u>	<u>18)</u>	<u>4)</u>	<u>5)</u>			1)		(0.01	(0.6		146	)		<u>(48)</u>	<u>3</u>		9	3	5	
									)	<u>31)</u>		14.8				(			2	6	
	<u>n</u>											(0.1	<del>2</del>			1					
	<u>≡</u> 7											<u>6)</u>				<u>3</u>					
	2															)					
	)																				
<del>20</del> <u>1.9</u>	5.9	84.0	1.1	0.48	0.70	0-1	-	<u></u>	<del>θ.</del>		θ.	, f	).1 <i>(</i> )	0.2	634	0.37	<del>0.</del>	θ.			4
<del>18</del> <u>95</u>	9	.08	(0.1	<u>6</u>	<u>04</u>	5 <u>.0</u>	0.2	0.		0.	3	e			<u>(27</u>	<u>144</u>	2	4	0.	0.	
<u>20</u> (0.2	(0.0	(0.2	)	(0.0)	(0.0	<u>(0.</u>	<u> </u>	15	2	3	3		0	(1.6	)	<u>(8)</u>	8	6	2	3	
<u>(n</u> 4 <u>00</u>	<u>5)</u>	)		)	<u>0)</u>	<u>0)</u>	8.5			4				)					3	6	
<u>=2</u> <u>9)</u>							<u>(2.</u>														
<u>4)</u>							<u>6)</u>														
2019	0. 0.	0 0.6	0	_ A	.3 -	- 0.0	52	0.	0.12			0.4	0. 0.1	4 <del>0.</del>	0.	-0.4	ρ				
	2 8	9	4 0.2				-	05					4	. 5	3	0	-				
	1		6 4	3	4	3							2	4	3						
				7	0																

The correlation while controlling for global radiation (Rg)

Inserted Cells	
Inserted Cells	

Deleted Cells
Deleted Cells
Inserted Cells
Inserted Cells

<sup>\*\*</sup> Based on daily values



Appendix figure 1. Soil water content at the study site (blue) and SMEAR Estonia station (red)

#### Appendix D. Estimation of NEE, GPP and ER from carbon budget data

For comparison with eddy-covariance estimates, net ecosystem exchange (NEE) from the biometric, inventory-based carbon budget was obtained as the negative of net ecosystem production (NEP):

$$NEE = -NEP$$

Gross primary production (GPP) and total ecosystem respiration (ER) were derived from annual net primary production (NPP) and heterotrophic respiration (R<sub>h</sub>) estimates using a fixed autotrophic respiration fraction. Autotrophic respiration (R<sub>n</sub>) was assumed to represent 57% of GPP, following the synthesis of boreal and temperate forest carbon budgets by Lindroth et al. (2020). Under this assumption, NPP can be expressed as:

$$NPP = GPP - R_a = (1 - a) \times GPP$$

where a is the fractional contribution of autotrophic respiration to GPP (here a=0.57). GPP was therefore calculated as:

$$GPP = \frac{NPP}{1 - a}$$

Autotrophic respiration was then obtained as:

060

070

 $R_a = a \times GPP$ 

Total ecosystem respiration was computed as:

$$ER = R_h + R_a$$

NEP from the carbon budget was then used as a consistency check:

$$NEP = GPP - ER$$

## Appendix E. Contribution of N2O and CH4 to the CO2-based global warming potential of the mature alder forest

Table E1. The annual balance of the alder forest in 2018 and 2019 expressed in CO<sub>2</sub>-eq. (GWP100 = 1 for CO<sub>2</sub>, GWP100=27.9 for CH<sub>4</sub> and GWP100 = 273 for N<sub>2</sub>O; IPCC 2021).

Gas	Method	2018	2019	Average	% from	Reference		
					CO <sub>2</sub>			
CO <sub>2</sub>	EC	<u>-2430</u>	<u>-1818</u>	<u>-2124</u>		This study		
$\underline{\text{CH}_4}$	<u>EC</u>	-1.60	<u>-3.57</u>	<u>-2.59</u>	0.1	(Mander et al., 2022)		
	Chambers	-2.03	-3.41	<u>-2.72</u>	0.1			
$N_2O$	<u>EC</u>	20.85	26.69	23.77	<u>1.1</u>	(Mander et al., 2021)		
	<u>Chambers</u>	147.08	<u>189.61</u>	168.35	<u>7.9</u>			

#### Data availability

The data are available upon request from the authors.

#### 1080 Author contribution

Article conceptualization was done by AK-with the help of KS and ÜM; data calculation and processing were performed by AK with valuable input from SR and DK; KS and ÜM acquired the funding and managed the Agali site; AK prepared the figures and wrote the article with editorial contributions from all authors.

#### Competing interests

1085 The authors declare that they have no conflict of interest.

#### Acknowledgements

This-The authors would like to thank Anonymous Reviewer #1 and Samuli Launiainen for their valuable suggestions, which allowed us to improve the study significantly. The research was supported by the Estonian Research Council (projects IUT2-16, PRG-352 and PRG2032)<sub>52</sub> the European Union Horizon programme under grant agreement No 101079192 (MLTOM23003R)<sub>52</sub> and the European Research Council (ERC) under grant agreementagreements No 101096403 (MLTOM23415R)<sub>52</sub> and No 101160308.

#### References

- Allen, C. D., Macalady, A. K., Chenchouni, H., Bachelet, D., McDowell, N., Vennetier, M., Kitzberger, T., Rigling, A., Breshears, D. D., Hogg, E. H. (Ted), Gonzalez, P., Fensham, R., Zhang, Z., Castro, J., Demidova, N., Lim, J.-H., Allard, G., Running, S. W., Semerci, A., and Cobb, N.: A global overview of drought and heat-induced tree mortality reveals emerging climate change risks for forests, For. Ecol. Manag., 259, 660–684, https://doi.org/10.1016/j.foreco.2009.09.001, 2010.
  - Allen, R. G., Pereira, L. S., Raes, D., and Smith, M.: Crop evapotranspiration: guidelines for computing crop water requirements, Food and Agriculture Organization of the United Nations, Rome, 300 pp., 1998.
  - Amiro, B.: Measuring boreal forest evapotranspiration using the energy balance residual, J. Hydrol., 366, 112–118, https://doi.org/10.1016/j.jhydrol.2008.12.021, 2009.
    - Anderegg, W. R. L., Schwalm, C., Biondi, F., Camarero, J. J., Koch, G., Litvak, M., Ogle, K., Shaw, J. D., Shevliakova, E., Williams, A. P., Wolf, A., Ziaco, E., and Pacala, S.: Pervasive drought legacies in forest ecosystems and their implications for carbon cycle models, Science, 349, 528–532, https://doi.org/10.1126/science.aab1833, 2015.
- Angert, A., Biraud, S., Bonfils, C., Henning, C. C., Buermann, W., Pinzon, J., Tucker, C. J., and Fung, I.: Drier summers cancel out the CO2 uptake enhancement induced by warmer springs, Proc. Natl. Acad. Sci., 102, 10823–10827, https://doi.org/10.1073/pnas.0501647102, 2005.
  - Aosaar, J., Varik, M., and Uri, V.: Biomass production potential of grey alder (Alnus incana (L.) Moench.) in Scandinavia and Eastern Europe: A review, Biomass Bioenergy, 45, 11–26, https://doi.org/10.1016/j.biombioe.2012.05.013, 2012.
- Arain, M. A., Xu, B., Brodeur, J. J., Khomik, M., Peichl, M., Beamesderfer, E., Restrepo-Couple, N., and Thorne, R.: Heat and drought impact on carbon exchange in an age-sequence of temperate pine forests, Ecol. Process., 11, 7, https://doi.org/10.1186/s13717-021-00349-7, 2022.
  - Aubinet, M., Vesala, T., and Papale, D. (Eds.): Eddy covariance: A practical guide to measurement and data analysis, Springer Netherlands, Dordrecht, https://doi.org/10.1007/978-94-007-2351-1, 2012.
- Baldocchi, D.: Measuring fluxes of trace gases and energy between ecosystems and the atmosphere the state and future of the eddy covariance method, Glob. Change Biol., 20, 3600–3609, https://doi.org/10.1111/gcb.12649, 2014.
  - Bastos, A., Ciais, P., Friedlingstein, P., Sitch, S., Pongratz, J., Fan, L., Wigneron, J. P., Weber, U., Reichstein, M., Fu, Z., Anthoni, P., Arneth, A., Haverd, V., Jain, A. K., Joetzjer, E., Knauer, J., Lienert, S., Loughran, T., McGuire, P. C., Tian, H.,

- Viovy, N., and Zaehle, S.: Direct and seasonal legacy effects of the 2018 heat wave and drought on European ecosystem productivity, Sci. Adv., 6, eaba2724, https://doi.org/10.1126/sciadv.aba2724, 2020.
- Beer, C., Ciais, P., Reichstein, M., Baldocchi, D., Law, B. E., Papale, D., Soussana, J.-F., Beamesderfer, E. R., Arain, M. A., Ammann, C., Buchmann, N., Frank, D., Gianelle, D., Janssens, I. A., Knohl, A., Köstner, B., Moors, E., Roupsard, O., Verbeeck, H., Vesala, T., Williams, C. A., and Wohlfahrt, G.: Temporal and among-site variability of inherent water use efficiency at the ecosystem level, Glob. Biogeochem. Cycles, 23, https://doi.org/10.1029/2008GB003233, 2009.
  - Khomik, M., and Brodeur, J. J.: The impact of seasonal and annual climate variations on the carbon uptake capacity of a
- 125 deciduous forest within the great lakes region of Canada, J.—Geophys. Res.—Biogeosciences, 125, e2019JG005389, https://doi.org/10.1029/2019JG005389\_2020.
  - Benson, D. R.: Isolation of frankia strains from alder actinorhizal root nodules, Appl. Environ. Microbiol., 44, 461–465, https://doi.org/10.1128/aem.44.2.461-465.1982, 1982.
  - Boese, S., Jung, M., Carvalhais, N., Teuling, A. J., and Reichstein, M.: Carbon—water flux coupling under progressive drought, Biogeosciences, 16, 2557–2572, https://doi.org/10.5194/bg-16-2557-2019, 2019.
    - Bréda, N., Huc, R., Granier, A., and Dreyer, E.: Temperate forest trees and stands under severe drought: a review of ecophysiological responses, adaptation processes and long-term consequences, Ann. For. Black, T. A., Chen, W. J., Barr, A. G., Sci., 63, 625–644, https://doi.org/10.1051/forest:2006042, 2006.
    - Arain, M.-A., Chen, Z., Nesic, Z., Hogg, E. H., Neumann, H. H., and Yang, P. C.: Increased carbon sequestration by a boreal
- deciduous forest in years with a warm spring, Geophys. Res. Lett., 27, 1271–1274, https://doi.org/10.1029/1999GL011234,
  - Bonan, G. B.: Forests and climate change: forcings, feedbacks, and the climate benefits of forests, Science, 320, 1444–1449, https://doi.org/10.1126/science.1155121, 2008.
- Breshears, D. D., Cobb, N. S., Rich, P. M., Price, K. P., Allen, C. D., Balice, R. G., Romme, W. H., Kastens, J. H., Floyd, M. L., Belnap, J., Anderson, J. J., Myers, O. B., and Meyer, C. W.: Regional vegetation die-off in response to global-change-type drought, Proc. Natl. Acad. Sci., 102, 15144–15148, https://doi.org/10.1073/pnas.0505734102, 2005.
  - Brodribb, T. J., Powers, J., Cochard, H., and Choat, B.: Hanging by a thread? Forests and drought, Science, 368, 261–266, https://doi.org/10.1126/science.aat7631, 2020.
- Brümmer, C., Black, T. A., Jassal, R. S., Grant, N. J., Spittlehouse, D. L., Chen, B., Nesic, Z., Amiro, B. D., Arain, M. A.,
  1145 Barr, A. G., Bourque, C. P.-A., Coursolle, C., Dunn, A. L., Flanagan, L. B., Humphreys, E. R., Lafleur, P. M., Margolis, H.
  A., McCaughey, J. H., and Wofsy, S. C.: How climate and vegetation type influence evapotranspiration and water use
  efficiency in Canadian forest, peatland and grassland ecosystems, Agric. For. Meteorol., 153, 14–30,
  https://doi.org/10.1016/j.agrformet.2011.04.008, 2012.
- Buras, A., Rammig, A., and Zang, C. S.: Quantifying impacts of the 2018 drought on European ecosystems in comparison to 2003, Biogeosciences, 17, 1655–1672, https://doi.org/10.5194/bg-17-1655-2020, 2020.
  - Butterbach-Bahl, K., Baggs, E. M., Dannenmann, M., Kiese, R., and Zechmeister-Boltenstern, S.: Nitrous oxide emissions from soils: how well do we understand the processes and their controls?, Philos. Trans. R. Soc. B Biol. Sci., 368, 20130122, https://doi.org/10.1098/rstb.2013.0122, 2013.
- Capon, S. J., Chambers, L. E., Mac Nally, R., Naiman, R. J., Davies, P., Marshall, N., Pittock, J., Reid, M., Capon, T., Douglas,
   M., Catford, J., Baldwin, D. S., Stewardson, M., Roberts, J., Parsons, M., and Williams, S. E.: Riparian ecosystems in the 21st century: Hotspots for climate change adaptation?, Ecosystems, 16, 359–381, https://doi.org/10.1007/s10021-013-9656-1, 2013.
  - Caudullo, G., Welk, E., and San-Miguel-Ayanz, J.: Chorological maps for the main European woody species, Data Brief, 12, 662–666, https://doi.org/10.1016/j.dib.2017.05.007, 2017.
- 1160 Cavin, L., Mountford, E. P., Peterken, G. F., and Jump, A. S.: Extreme drought alters competitive dominance within and between tree species in a mixed forest stand, Funct. Ecol., 27, 1424–1435, https://doi.org/10.1111/1365-2435.12126, 2013.
  - Chen, L., Keski-Saari, S., Kontunen-Soppela, S., Zhu, X., Zhou, X., Hänninen, H., Pumpanen, J., Mola-Yudego, B., Wu, D., and Berninger, F.: Immediate and carry-over effects of late-spring frost and growing season drought on forest gross primary productivity capacity in the Northern Hemisphere, Glob. Change Biol., n/a, https://doi.org/10.1111/gcb.16751, 2023.
- 1165 Chi, J., Nilsson, M. B., Kljun, N., Wallerman, J., Fransson, J. E. S., Laudon, H., Lundmark, T., and Peichl, M.: The carbon balance of a managed boreal landscape measured from a tall tower in northern Sweden, Agric. For. Meteorol., 274, 29–41, https://doi.org/10.1016/j.agrformet.2019.04.010, 2019.
  - Fischer Davidson, E. A., Keller, M., Sippel, SErickson, H. E., Verchot, L. V., and Knutti, R.: Increasing probability Veldkamp, E.: Testing a Conceptual Model of record-shattering climate extremes, Nat. Soil Emissions of Nitrous and Nitric Oxides,

- BioScience, 50, 667–680 Clim. Change, 11, 689–695, https://doi.org/10.1038/s41558-021-01092-9, 2021\_1641/0006-3568(2000)050[0667:TACMOS]2.0.CO;2, 2000.
  - Dlugokencky, E. J., Nisbet, E. <u>G., Frank</u>Fisher, R., and Lowry, D.: Global atmospheric methane: budget, changes and dangers, Philos. Trans. R. Soc. Math. Phys. Eng. Sci., 369, 2058–2072, https://doi.org/10.1098/rsta.2010.0341, 2011.
- Doughty, C. E., Malhi, Y., Araujo-Murakami, A., Metcalfe, D. B., Silva-Espejo, J. E., Arroyo, L., Heredia, J. P., Reichstein, Pardo-Toledo, E., Mendizabal, L. M., Bahn-Rojas-Landivar, V. D., Vega-Martinez, M., Thonicke, K., Frank, D., Maheeha-Flores-Valencia, M. D., Smith., Sibler-Rivero, R., Moreno-Vare, L., Viscarra, L. J., Chuviru-Castro, T., Osinaga-Becerra P., Velde, M., Vicea, S., Babst, and Ledezma, R.: Allocation trade-offs dominate the response of tropical forest growth to seasonal and interannual drought, Ecology, 95, 2192–2201, https://doi.org/10.1890/13-1507.1, 2014.
- Dybala, K. E., Matzek, V., Gardali, T., and Seavy F., Beer, C., Buchmann, N., Canadell, J. G., Ciais, P., Cramer, W., Ibrom, A., Miglietta, F., Poulter, B., Rammig, E.: Carbon sequestration in riparian forests: A., Seneviratne, S. I., Walz, A., Wattenbach, M., Zavala, M. A., and Zscheischler, J.: Effects of climate extremes on the terrestrial carbon cycle: concepts, processes and potential future impacts global synthesis and meta-analysis, Glob. Change Biol., 21, 2861–288025, 57–67, https://doi.org/10.1111/gcb.14475, 2019.
- Eschenbach, C. and Kappen, L.: Leaf water relations of black alder [Alnus glutinosa (L.) Gaertn.] growing at neighbouring sites with different water regimes, Trees, 14, 28–38, https://doi.org/10.1007/s004680050004, 1999.
  - Farquhar, G. D. and Sharkey, T. D.: Stomatal conductance and photosynthesis, Annu. Rev. Plant Physiol., 33, 317–345, https://doi.org/10.1146/annurev.pp.33.060182.001533, 1982.
- Feng, H., Guo, J., Han, M., Wang, W., Peng, C., Jin, J., Song, X., and Yu, S.: A review of the mechanisms and controlling factors of methane dynamics in forest ecosystems, For. Ecol. Manag., 455, 117702, https://doi.org/10.1016/j.foreco.2019.117702, 2020.
  - Fisher, J. B., Melton, F., Middleton, E., Hain, C., Anderson, M., Allen, R., McCabe, M. F., Hook, S., Baldocchi, D., Townsend, P. A., Kilic, A., Tu, K., Miralles, D. D., Perret, J., Lagouarde, J.-P., Waliser, D., Purdy, A. J., French, A., Schimel, D., Famiglietti, J. S., Stephens, G., and Wood, E. F.: The future of evapotranspiration: Global requirements for ecosystem functioning, carbon and climate feedbacks, agricultural management, and water resources, Water Resour. Res., 53, 2618–2626, https://doi.org/10.1002/2016WR020175, 2017.
  - Flanagan, L. B., Nikkel, D. J., Scherloski, L. M., Tkach, R. E., Smits, K. M., Selinger, L. B., and Rood, S. B.: Multiple processes contribute to methane emission in a riparian cottonwood forest ecosystem, New Phytol., 229, 1970–1982, https://doi.org/10.1111/nph.16977, 2021.
- Fleischer, K., Rebel, K. T., van der Molen, M. K., Erisman, J. W., Wassen, M. J., van Loon, E. E., Montagnani, L., Gough, C. M., Herbst, M., Janssens, I. A., 12916, 2015 Gianelle, D., and Dolman, A. J.: The contribution of nitrogen deposition to the photosynthetic capacity of forests, Glob. Biogeochem. Cycles, 27, 187–199, https://doi.org/10.1002/gbc.20026, 2013.
  - Foken, T.: The energy balance closure problem: an overview, Ecol. Appl., 18, 1351–1367, https://doi.org/10.1890/06-0922.1, 2008.
- Friedlingstein, P., O'Sullivan, M., Jones, M. W., Andrew, R. M., Gregor, L., Hauck, J., Le Quéré, C., Luijkx, I. T., Olsen, A., 1205 Peters, G. P., Peters, W., Pongratz, J., Schwingshackl, C., Sitch, S., Canadell, J. G., Ciais, P., Jackson, R. B., Alin, S. R., Alkama, R., Arneth, A., Arora, V. K., Bates, N. R., Becker, M., Bellouin, N., Bittig, H. C., Bopp, L., Chevallier, F., Chini, L. P., Cronin, M., Evans, W., Falk, S., Feely, R. A., Gasser, T., Gehlen, M., Gkritzalis, T., Gloege, L., Grassi, G., Gruber, N., Gürses, Ö., Harris, I., Hefner, M., Houghton, R. A., Hurtt, G. C., Iida, Y., Ilyina, T., Jain, A. K., Jersild, A., Kadono, K., Kato, E., Kennedy, D., Klein Goldewijk, K., Knauer, J., Korsbakken, J. I., Landschützer, P., Lefèvre, N., Lindsay, K., Liu, J., Liu,
- Z., Marland, G., Mayot, N., McGrath, M. J., Metzl, N., Monacci, N. M., Munro, D. R., Nakaoka, S.-I., Niwa, Y., O'Brien, K., Ono, T., Palmer, P. I., Pan, N., Pierrot, D., Pocock, K., Poulter, B., Resplandy, L., Robertson, E., Rödenbeck, C., Rodriguez, C., Rosan, T. M., Schwinger, J., Séférian, R., Shutler, J. D., Skjelvan, I., Steinhoff, T., Sun, Q., Sutton, A. J., Sweeney, C., Takao, S., Tanhua, T., Tans, P. P., Tian, X., Tian, H., Tilbrook, B., Tsujino, H., Tubiello, F., van der Werf, G. R., Walker, A. P., Wanninkhof, R., Whitehead, C., Willstrand Wranne, A., et al.: Global Carbon Budget 2022, Earth Syst. Sci. Data, 14, 1215
  4811–4900, https://doi.org/10.5194/essd-14-4811-2022, 2022.
  - Fu, Z., Ciais, P., Bastos, A., Stoy, P. C., Yang, H., Green, J. K., Wang, B., Yu, K., Huang, Y., Knohl, A., Šigut, L., Gharun, M., Cuntz, M., Arriga, N., Roland, M., Peichl, M., Migliavacca, M., Cremonese, E., Varlagin, A., Brümmer, C., Gourlez de la Motte, L., Fares, S., Buchmann, N., El-Madany, T. S., Pitacco, A., Vendrame, N., Li, Z., Vincke, C., Magliulo, E., and Koebsch, F.: Sensitivity of gross primary productivity to climatic drivers during the summer drought of 2018 in Europe, Philos. Trans. R. Soc. B Biol. Sci., 375, 20190747, https://doi.org/10.1098/rstb.2019.0747, 2020.
  - Gao, Y., Markkanen, T., Aurela, M., Mammarella, I., Thum, T., Tsuruta, A., Yang, H., and Aalto, T.: Response of water use efficiency to summer drought in a boreal Scots pine forest in Finland, Biogeosciences, 14, 4409–4422, https://doi.org/10.5194/bg-14-4409-2017, 2017.
- Ge, Z.-M., Kellomäki, S., Zhou, X., and Peltola, H.: The role of climatic variability in controlling carbon and water budgets in a boreal Scots pine forest during ten growing seasons, Boreal Environ. Res., 19, 181–194, 2014.

- Gilmanov, T. G., Verma, S. B., Sims, P. L., Meyers, T. P., Bradford, J. A., Burba, G. G., and Suyker, A. E.: Gross primary production and light response parameters of four Southern Plains ecosystems estimated using long-term CO2-flux tower measurements, Glob. Biogeochem. Cycles, 17, https://doi.org/10.1029/2002GB002023, 2003.
- Gonsamo, A., Chen, J. M., and D'Odorico, P.: Deriving land surface phenology indicators from CO2 eddy covariance measurements, Ecol. Indic., 29, 203–207, https://doi.org/10.1016/j.ecolind.2012.12.026, 2013.
  - Granier, A., Bréda, N., Longdoz, B., Gross, Green, J. K., Seneviratne, S. I., Berg, A. M., Findell, K. L., Hagemann, S., Lawrence, D. M., and Gentine, P.: Large influence of soil moisture on long-term terrestrial carbon uptake, Nature, 565, 476–479, https://doi.org/10.1038/s41586-018-0848-x, 2019.
  - P., and Ngao, J.: Ten years of fluxes and stand growth in a young beech forest at Hesse, North-eastern France, Ann. For. Sci.,
- 1235 65, 704 704, https://doi.org/10.1051/forest:2008052, 2008.
  - Gutierrez Lopez, J., Tor-ngern, P., Oren, R., Kozii, N., Laudon, H., and Hasselquist, N. J.: How tree species, tree size, and topographical location influenced tree transpiration in northern boreal forests during the historic 2018 drought, Glob. Change Biol., 27, 3066–3078, https://doi.org/10.1111/gcb.15601, 2021.
  - Haberstroh, S., Werner, C., Grün, M., Kreuzwieser, J., Seifert, T., Schindler, D., and Christen, A.: Central European 2018 hot drought shifts Scots pine forest to its tipping point, Plant Biol., 24, 1186–1197, https://doi.org/10.1111/plb.13455, 2022.
  - Hadden, D. and Grelle, A.: Changing temperature response of respiration turns boreal forest from carbon sink into carbon source, Agric. For. Meteorol., 223, 30–38, https://doi.org/10.1016/j.agrformet.2016.03.020, 2016.
  - Hari, V., Rakovec, O., Markonis, Y., Hanel, M., and Kumar, R.: Increased future occurrences of the exceptional 2018–2019 Central European drought under global warming, Sci. Rep., 10, 12207, https://doi.org/10.1038/s41598-020-68872-9, 2020.
- 1245 Harris, N. L., Gibbs, D. A., Baccini, A., Birdsey, R. A., de Bruin, S., Farina, M., Fatoyinbo, L., Hansen, M. C., Herold, M., Houghton, R. A., Potapov, P. V., Suarez, D. R., Roman-Cuesta, R. M., Saatchi, S. S., Slay, C. M., Turubanova, S. A., and Tyukavina, A.: Global maps of twenty-first century forest carbon fluxes, Nat. Clim. Change, 11, 234–240, https://doi.org/10.1038/s41558-020-00976-6, 2021.
- Hikino, K., Danzberger, J., Riedel, V. P., Hesse, B. D., Hafner, B. D., Gebhardt, T., Rehschuh, R., Ruehr, N. K., Brunn, M.,
   Bauerle, T. L., Landhäusser, S. M., Lehmann, M. M., Rötzer, T., Pretzsch, H., Buegger, F., Weikl, F., Pritsch, K., and Grams, T. E. E.: Dynamics of initial carbon allocation after drought release in mature Norway spruce—Increased belowground allocation of current photoassimilates covers only half of the carbon used for fine-root growth, Glob. Change Biol., 28, 6889–6905, https://doi.org/10.1111/gcb.16388, 2022.
  - Houle, D., Lajoie, G., and Duchesne, L.: Major losses of nutrients following a severe drought in a boreal forest, Nat. Plants, 2, 16187, https://doi.org/10.1038/nplants.2016.187, 2016.
    - Huang, M., Piao, S., Sun, Y., Ciais, P., Cheng, L., Mao, J., Poulter, B., Shi, X., Zeng, Z., and Wang, Y.: Change in terrestrial ecosystem water-use efficiency over the last three decades, Glob. Change Biol., 21, 2366–2378, https://doi.org/10.1111/gcb.12873, 2015.
- Huth, V., Hoffmann, M., Bereswill, S., Zak, D., and Augustin, J.: The climate warming effect of a fen peat meadow with fluctuating water table is reduced by young alder trees, Mires Peat, 1–18, https://doi.org/10.19189/MaP.2017.OMB.291, 2018.
  - Jarvis, P. J.: Coupling of carbon and water interactions in forest stands, Tree Physiol., 2, 347–368, https://doi.org/10.1093/treephys/2.1-2-3.347, 1986.
- Jassal, R. S., Black, T. A., Spittlehouse, D. L., Brümmer, C., and Nesic, Z.: Evapotranspiration and water use efficiency in different-aged Pacific Northwest Douglas-fir stands, Agric. For. Meteorol., 149, 1168–1178, https://doi.org/10.1016/j.agrformet.2009.02.004, 2009.
  - Jin, C., Zha, T., Bourque, C. P.-A., Liu, P., Jia, X., Zhang, F., Yu, H., Tian, Y., Li, X., Kang, X., Guo, X., and Wang, N.: Multi-year trends and interannual variation in ecosystem resource use efficiencies in a young mixedwood plantation in northern China, Agric. For. Meteorol., 330, 109318, https://doi.org/10.1016/j.agrformet.2023.109318, 2023.
- Kannenberg, S. A., Maxwell, J. T., Pederson, N., D'Orangeville, L., Ficklin, D. L., and Phillips, R. P.: Drought legacies are dependent on water table depth, wood anatomy and drought timing across the eastern US, Ecol. Lett., 22, 119–127, https://doi.org/10.1111/ele.13173, 2019.
  - Kannenberg, S. A., Schwalm, C. R., and Anderegg, W. R. L.: Ghosts of the past: how drought legacy effects shape forest functioning and carbon cycling, Ecol. Lett., 23, 891–901, https://doi.org/10.1111/ele.13485, 2020.
- Kannenberg, S. A., Anderegg, W. R. L., Barnes, M. L., Dannenberg, M. P., and Knapp, A. K.: Dominant role of soil moisture
   in mediating carbon and water fluxes in dryland ecosystems, Nat. Geosci., 17, 38–43, https://doi.org/10.1038/s41561-023-01351-8, 2024.
  - Keenan, T. F., Hollinger, D. Y., Bohrer, G., Dragoni, D., Munger, J. W., Schmid, H. P., and Richardson, A. D.: Increase in forest water-use efficiency as atmospheric carbon dioxide concentrations rise, Nature, 499, 324–327, https://doi.org/10.1038/nature12291, 2013.

- 1280 Keenan, T. F., Gray, J., Friedl, M. A., Toomey, M., Bohrer, G., Hollinger, D. Y., Munger, J. W., O'Keefe, J., Schmid, H. P., Wing, I. S., Yang, B., and Richardson, A. D.: Net carbon uptake has increased through warming-induced changes in temperate forest phenology, Nat. Clim. Change, 4, 598–604, https://doi.org/10.1038/nclimate2253, 2014.
- Kibler, C. L., Schmidt, E. C., Roberts, D. A., Stella, J. C., Kui, L., Lambert, A. M., and Singer, M. B.: A brown wave of riparian woodland mortality following groundwater declines during the 2012–2019 California drought, Environ. Res. Lett., 16, 084030, https://doi.org/10.1088/1748-9326/ac1377, 2021.
  - Kljun, N., Black, T. A., Griffis, T. J., Barr, A. G., Gaumont-Guay, D., Morgenstern, K., McCaughey, J. H., and Nesic, Z.: Response of net ecosystem productivity of three boreal forest stands to drought, Ecosystems, 9, 1128–1144, https://doi.org/10.1007/s10021-005-0082-x, 2006.
  - Kljun, N., Calanca, P., Rotach, M. W., and Schmid, H. P.: A simple two-dimensional parameterisation for Flux Footprint
- 1290 Prediction (FFP), Geosci. Model Dev., 8, 3695-3713, https://doi.org/10.5194/gmd-8-3695-2015, 2015.
  - Kochendorfer, J., Castillo, E. G., Haas, E., Oechel, W. C., and Paw U., K. T.: Net ecosystem exchange, evapotranspiration and canopy conductance in a riparian forest, Agric. For. Meteorol., 151, 544–553, https://doi.org/10.1016/j.agrformet.2010.12.012, 2011.
- Kowalska, N., Šigut, L., Stojanović, M., Fischer, M., Kyselova, I., and Pavelka, M.: Analysis of floodplain forest sensitivity to drought, Philos. Trans. R. Soc. B Biol. Sci., 375, 20190518, https://doi.org/10.1098/rstb.2019.0518, 2020.
  - Kozlowski, T. T.: Responses of woody plants to flooding and salinity, Tree Physiol., 17, 490 https://doi.org/10.1093/treephys/17.7.490, 1997.
  - Krasnova, A., Mander, Ü., Noe, S. M., Uri, V., Krasnov, D., and Soosaar, K.: Hemiboreal forests' CO2 fluxes response to the European 2018 heatwave, Agric. For. Meteorol., 323, 109042, https://doi.org/10.1016/j.agrformet.2022.109042, 2022.
- 300 Krishnan, P., Black, T. A., Grant, N. J., Barr, A. G., Hogg, E. (Ted) H., Jassal, R. S., and Morgenstern, K.: Impact of changing soil moisture distribution on net ecosystem productivity of a boreal aspen forest during and following drought, Agric. For. Meteorol., 139, 208–223, https://doi.org/10.1016/j.agrformet.2006.07.002, 2006.
- Krzaklewski, W., Pietrzykowski, M., and Woś, B.: Survival and growth of alders (Alnus glutinosa (L.) Gaertn. and Alnus incana (L.) Moench) on fly ash technosols at different substrate improvement, Ecol. Eng., 49, 35–40, https://doi.org/10.1016/j.ecoleng.2012.08.026, 2012.
  - KupperLauniainen, S., Katul, G. G., Leppä, K., Kolari, P., Sõber, J., Sellin, A., Lõhmus, K., Tullus, A., Räim, O., Lubenets, K., TulvaAslan, T., Grönholm, T., Korhonen, L., Mammarella, I., Uri, V., Zobel, M., Kull, O., and Sõber, A.: An experimental facility for free air humidity manipulation (FAHM) can alter water flux through deciduous tree canopy, Environ. Exp. Bot., 72, 432–438, https://doi.org/10.1016/j.envexpbot.2010.09.003, 2011.
- 310 Kutsch, W. L., Liu, C., Hormann, G., and Herbst, M.: Spatial heterogeneity of ecosystem Vesala, T.: Does growing atmospheric CO2 explain increasing carbon fluxessink in a broadleavedboreal coniferous forest in Northern Germany,?, Glob. Change Biol., 11, 70 88n/a, https://doi.org/10.1111/j.1365-2486.2004.00884.x, 2005gcb.16117, 2022.
  - Lindroth, A., Grelle, A., and Morén, A.: Long-term measurements of boreal forest carbon balance reveal large temperature sensitivity, Glob. Change Biol., 4, 443–450, https://doi.org/10.1046/j.1365-2486.1998.00165.x, 1998.
- Lindroth, A., Holst, J., Linderson, M.-L., Aurela, M., Biermann, T., Heliasz, M., Chi, J., Ibrom, A., Kolari, P., Klemedtsson, L., Krasnova, A., Laurila, T., Lehner, I., Lohila, A., Mammarella, I., Mölder, M., Löfvenius, M. O., Peichl, M., Pilegaard, K., Soosaar, K., Vesala, T., Vestin, P., Weslien, P., and Nilsson, M.: Effects of drought and meteorological forcing on carbon and water fluxes in Nordic forests during the dry summer of 2018, Philos. Trans. R. Soc. B Biol. Sci., 375, 20190516, https://doi.org/10.1098/rstb.2019.0516, 2020.
- 320 Lloyd, J.Lloret, F., Keeling, E. G., and Taylor, J.Sala, A.: On the temperature dependence Components of soil respiration, Funct. Ecol., 8, 315tree resilience: effects of successive low-growth episodes in old ponderosa pine forests, Oikos, 120, 1909–1920, https://doi.org/10.2307/2389824, 19941111/j.1600-0706.2011.19372.x, 2011.
  - Mander, Ü., Lõhmus, K., Teiter, S., Uri, V., and Augustin, J.: Gaseous nitrogen and carbon fluxes in riparian alder stands, Boreal Environ. Res., 13, 231–241, 2008.
- Mander, Ü., Krasnova, A., Escuer-Gatius, J., Espenberg, M., Schindler, T., Machacova, K., Pärn, J., Maddison, M., Megonigal, J. P., Pihlatie, M., Kasak, K., Niinemets, Ü., Junninen, H., and Soosaar, K.: Forest canopy mitigates soil N2O emission during hot moments, Npj Clim. Atmospheric Sci., 4, 39, https://doi.org/10.1038/s41612-021-00194-7, 2021.
- Mander, Ü., Krasnova, A., Schindler, T., Megonigal, J. P., Escuer-Gatius, J., Espenberg, M., Machacova, K., Maddison, M., Pärn, J., Ranniku, R., Pihlatie, M., Kasak, K., Niinemets, Ü., and Soosaar, K.: Long-term dynamics of soil, tree stem and
- 1330 ecosystem methane fluxes in a riparian forest, Sci. Total Environ., 809, 151723, https://doi.org/10.1016/j.scitotenv.2021.151723, 2022.

- Massmann, A., Gentine, P., and Lin, C.: When Does Vapor Pressure Deficit Drive or Reduce Evapotranspiration?, J. Adv. Model. Earth Syst., 11, 3305–3320, https://doi.org/10.1029/2019MS001790, 2019.
- Mauder, M., Genzel, S., Fu, J., Kiese, R., Soltani, M., Steinbrecher, R., Zeeman, M., Banerjee, T., De Roo, F., and Kunstmann,
   H.: Evaluation of energy balance closure adjustment methods by independent evapotranspiration estimates from lysimeters and hydrological simulations, Hydrol. Process., 32, 39–50, https://doi.org/10.1002/hyp.11397, 2018.
  - Mauder, M., Foken, T., and Cuxart, J.: Surface-energy-balance closure over land: a review, Bound.-Layer Meteorol., 177, 395–426, https://doi.org/10.1007/s10546-020-00529-6, 2020.
- McDowell, N., Pockman, W. T., Allen, C. D., Breshears, D. D., Cobb, N., Kolb, T., Plaut, J., Sperry, J., West, A., Williams, D. G., and Yepez, E. A.: Mechanisms of plant survival and mortality during drought: why do some plants survive while others succumb to drought?, New Phytol., 178, 719–739, https://doi.org/10.1111/j.1469-8137.2008.02436.x, 2008.
  - Michaelis, L. and Menten, M. L.: Die kinetik der invertinwirkung, Biochem Z, 49, 352, 1913
  - van der Molen, M. K., Dolman, A. J., Ciais, P., Eglin, T., Gobron, N., Law, B. E., Meir, P., Peters, W., Phillips, O. L., Reichstein, M., Chen, T., Dekker, S. C., Doubková, M., Friedl, M. A., Jung, M., van den Hurk, B. J. J. M., de Jeu, R. A. M., Kruijt, B., Ohta, T., Rebel, K. T., Plummer, S., Seneviratne, S. I., Sitch, S., Teuling, A. J., van der Werf, G. R., and Wang, G.: Drought and ecosystem carbon cycling, Agric. For. Meteorol., 151, 765–773, https://doi.org/10.1016/j.agrformet.2011.01.018, 2011.
- Musavi, T., Migliavacca, M., Reichstein, M., Kattge, J., Wirth, C., Black, T. A., Janssens, I., Knohl, A., Loustau, D., Roupsard, O., Varlagin, A., Rambal, S., Cescatti, A., Gianelle, D., Kondo, H., Tamrakar, R., and Mahecha, M. D.: Stand age and species richness dampen interannual variation of ecosystem-level photosynthetic capacity, Nat. Ecol. Evol., 1, 1–7, https://doi.org/10.1038/s41559-016-0048, 2017.
  - Naiman, R. J. and Décamps, H.: The ecology of interfaces: Riparian zones, Annu. Rev. Ecol. Syst., 28, 621–658, https://doi.org/10.1146/annurev.ecolsys.28.1.621, 1997.
- Ney, P., Graf, A., Bogena, H., Diekkrüger, B., Drüe, C., Esser, O., Heinemann, G., Klosterhalfen, A., Pick, K., Pütz, T., Schmidt, M., Valler, V., and Vereecken, H.: CO2 fluxes before and after partial deforestation of a Central European spruce forest, Agric. For. Meteorol., 274, 61–74, https://doi.org/10.1016/j.agrformet.2019.04.009, 2019.
  - Niu, X. and Liu, S.: Drought affected ecosystem water use efficiency of a natural oak forest in central china, Forests, 12, 839, https://doi.org/10.3390/f12070839, 2021.
- Novick, K. A., Ficklin, D. L., Stoy, P. C., Williams, C. A., Bohrer, G., Oishi, A. C., Papuga, S. A., Blanken, P. D., Noormets,
   A., Sulman, B. N., Scott, R. L., Wang, L., and Phillips, R. P.: The increasing importance of atmospheric demand for ecosystem water and carbon fluxes, Nat. Clim. Change, 6, 1023–1027, https://doi.org/10.1038/nclimate3114, 2016.
  - Oren, R., Sperry, J. S., Katul, G. G., Pataki, D. E., Ewers, B. E., Phillips, N., and Schäfer, K. V. R.: Survey and synthesis of intra- and interspecific variation in stomatal sensitivity to vapour pressure deficit, Plant Cell Environ., 22, 1515–1526, https://doi.org/10.1046/j.1365-3040.1999.00513.x, 1999.
- Pan, Y., Birdsey, R. A., Fang, J., Houghton, R., Kauppi, P. E., Kurz, W. A., Phillips, O. L., Shvidenko, A., Lewis, S. L., Canadell, J. G., Ciais, P., Jackson, R. B., Pacala, S. W., McGuire, A. D., Piao, S., Rautiainen, A., Sitch, S., and Hayes, D.: A large and persistent carbon sink in the world's forests, Science, 333, 988–993, https://doi.org/10.1126/science.1201609, 2011.
- Papale, D., Reichstein, M., Aubinet, M., Canfora, E., Bernhofer, C., Kutsch, W., Longdoz, B., Rambal, S., Valentini, R., Vesala, T., and Yakir, D.: Towards a standardized processing of Net Ecosystem Exchange measured with eddy covariance technique: algorithms and uncertainty estimation, Biogeosciences, 3, 571–583, https://doi.org/10.5194/bg-3-571-2006, 2006.
  - Piao, S., Wang, X., Park, T., Chen, C., Lian, X., He, Y., Bjerke, J. W., Chen, A., Ciais, P., Tømmervik, H., Nemani, R. R., and Myneni, R. B.: Characteristics, drivers and feedbacks of global greening, Nat. Rev. Earth Environ., 1, 14–27, https://doi.org/10.1038/s43017-019-0001-x, 2020.
- Pilegaard, K. and Ibrom, A.: Net carbon ecosystem exchange during 24 years in the Sorø Beech Forest relations to phenology and climate, Tellus B Chem. Phys. Meteorol., 72, 2020.
  - Pohl, F., Werban, U., Kumar, R., Hildebrandt, A., and Rebmann, C.: Observational evidence of legacy effects of the 2018 drought on a mixed deciduous forest in Germany, Sci. Rep., 13, 10863, https://doi.org/10.1038/s41598-023-38087-9, 2023.
  - Portela, A. P., Gonçalves, J. F., Durance, I., Vieira, C., and Honrado, J.: Riparian forest response to extreme drought is influenced by climatic context and canopy structure, Sci. Total Environ., 881, 163128, https://doi.org/10.1016/j.scitotenv.2023.163128, 2023.

1380

- Reichstein, M., Tenhunen, J. D., Roupsard, O., Ourcival, J., Rambal, S., Miglietta, F., Peressotti, A., Pecchiari, M., Tirone, G., and Valentini, R.: Severe drought effects on ecosystem CO2 and H2O fluxes at three Mediterranean evergreen sites: revision of current hypotheses?, Glob. Change Biol., 8, 999–1017, https://doi.org/10.1046/j.1365-2486.2002.00530.x, 2002.
- Rohde, M. M., Stella, J. C., Roberts, D. A., and Singer, M. B.: Groundwater dependence of riparian woodlands and the disrupting effect of anthropogenically altered streamflow, Proc. Natl. Acad. Sci. U. S. A., 118, e2026453118, https://doi.org/10.1073/pnas.2026453118, 2021.

- Rood, S. B., Pan, J., Gill, K. M., Franks, C. G., Samuelson, G. M., and Shepherd, A.: Declining summer flows of Rocky Mountain rivers: Changing seasonal hydrology and probable impacts on floodplain forests, J. Hydrol., 349, 397–410, https://doi.org/10.1016/j.jhydrol.2007.11.012, 2008.
- 1390 Rytter, L. and Rytter, R.-M.: Growth and carbon capture of grey alder (Alnus incana (L.) Moench.) under north European conditions Estimates based on reported research, For. Ecol. Manag., 373, 56–65, https://doi.org/10.1016/j.foreco.2016.04.034, 2016.
  - Rytter, L., 'Slapokas, T., and Granhall, U.: Woody biomass and litter production of fertilized grey alder plantations on a low-humified peat bog, For. Ecol. Manag., 28, 161–176, https://doi.org/10.1016/0378-1127(89)90001-7, 1989.
- l395 Schaaf, C. and Wang, Z.: MODIS/Terra+Aqua BRDF/Albedo Daily L3 Global 500m V061 https://doi.org/10.5067/MODIS/MCD43A3.061, 2021.
  - Schlesinger, W. H., Dietze, M. C., Jackson, R. B., Phillips, R. P., Rhoades, C. C., Rustad, L. E., and Vose, J. M.: Forest biogeochemistry in response to drought, Glob. Change Biol., 22, 2318–2328, https://doi.org/10.1111/gcb.13105, 2016.
- Schnabel, F., Purrucker, S., Schmitt, L., Engelmann, R. A., Kahl, A., Richter, R., Seele-Dilbat, C., Skiadaresis, G., and Wirth,

  C.: Cumulative growth and stress responses to the 2018–2019 drought in a European floodplain forest, Glob. Change Biol.,
  28, 1870–1883, https://doi.org/10.1111/gcb.16028, 2022.
  - Schwalm, C. R., Anderegg, W. R. L., Michalak, A. M., Fisher, J. B., Biondi, F., Koch, G., Litvak, M., Ogle, K., Shaw, J. D., Wolf, A., Huntzinger, D. N., Schaefer, K., Cook, R., Wei, Y., Fang, Y., Hayes, D., Huang, M., Jain, A., and Tian, H.: Global patterns of drought recovery, Nature, 548, 202–205, https://doi.org/10.1038/nature23021, 2017.
- 405 Scott, R. L., Edwards, E. A., Shuttleworth, W. J., Huxman, T. E., Watts, C., and Goodrich, D. C.: Interannual and seasonal variation in fluxes of water and carbon dioxide from a riparian woodland ecosystem, Agric. For. Meteorol., 122, 65–84, https://doi.org/10.1016/j.agrformet.2003.09.001, 2004.
  - Senf, C. and Seidl, R.: Persistent impacts of the 2018 drought on forest disturbance regimes in Europe, Biogeosciences, 18, 5223–5230, https://doi.org/10.5194/bg-18-5223-2021, 2021.
- 1410 Singer, M. B., Stella, J. C., Dufour, S., Piégay, H., Wilson, R. J. S., and Johnstone, L.: Contrasting water-uptake and growth responses to drought in co-occurring riparian tree species, Ecohydrology, 6, 402–412, https://doi.org/10.1002/eco.1283, 2013.
  - Singer, M. B., Sargeant, C. I., Piégay, H., Riquier, J., Wilson, R. J. S., and Evans, C. M.: Floodplain ecohydrology: Climatic, anthropogenic, and local physical controls on partitioning of water sources to riparian trees, Water Resour. Res., 50, 4490–4513, https://doi.org/10.1002/2014WR015581, 2014.
- Smith, N. E., Kooijmans, L. M. J., Koren, G., van Schaik, E., van der Woude, A. M., Wanders, N., Ramonet, M., Xueref-Remy, I., Siebicke, L., Manca, G., Brümmer, C., Baker, I. T., Haynes, K. D., Luijkx, I. T., and Peters, W.: Spring enhancement and summer reduction in carbon uptake during the 2018 drought in northwestern Europe, Philos. Trans. R. Soc. B Biol. Sci., 375, 20190509, https://doi.org/10.1098/rstb.2019.0509, 2020.
- Soosaar, K., Mander, Ü., Maddison, M., Kanal, A., Kull, A., Lõhmus, K., Truu, J., and Augustin, J.: Dynamics of gaseous nitrogen and carbon fluxes in riparian alder forests, Ecol. Eng., 37, 40–53, https://doi.org/10.1016/j.ecoleng.2010.07.025, 2011.
  - Stella, J. C., Riddle, J., Piégay, H., Gagnage, M., and Trémélo, M.-L.: Climate and local geomorphic interactions drive patterns of riparian forest decline along a Mediterranean Basin river, Geomorphology, 202, 101–114, https://doi.org/10.1016/j.geomorph.2013.01.013, 2013.
- 425 Thomas, C. K., Law, B. E., Irvine, J., Martin, J. G., Pettijohn, J. C., and Davis, K. J.: Seasonal hydrology explains interannual and seasonal variation in carbon and water exchange in a semiarid mature ponderosa pine forest in central Oregon, J. Geophys.
  <u>Res.</u> Teskey, R., Wertin, T., Bauweraerts, I., Ameye, M., Meguire, MBiogeosciences, 114, <a href="https://doi.org/10.1029/2009JG001010">https://doi.org/10.1029/2009JG001010</a>, 2009.
  - -A., and Steppe, K.: Responses of tree species to heat waves and extreme heat events, Plant Cell Environ., 38, 1699-1712,
- 430 https://doi.org/10.1111/pce.12417, 2015.
  - Trenberth, K. E., Dai, A., van der Schrier, G., Jones, P. D., Barichivich, J., Briffa, K. R., and Sheffield, J.: Global warming and changes in drought, Nat. Clim. Change, 4, 17–22, https://doi.org/10.1038/nclimate2067, 2014.
  - Uri, V., Aosaar, J., Varik, M., Becker, H., Ligi, K., Padari, A., Kanal, A., and Lõhmus, K.: The dynamics of biomass production, carbon and nitrogen accumulation in grey alder (Alnus incana (L.) Moench) chronosequence stands in Estonia,
- 435 For. Ecol. Manag., 327, 106-117, https://doi.org/10.1016/j.foreco.2014.04.040, 2014.
  - Uri, V., Kukumägi, M., Aosaar, J., Varik, M., Becker, H., Soosaar, K., Morozov, G., Ligi, K., Padari, A., Ostonen, I., and Karoles, K.: Carbon budgets in fertile grey alder (Alnus incana (L.) Moench.) stands of different ages, For. Ecol. Manag., 396, 55–67, https://doi.org/10.1016/j.foreco.2017.04.004, 2017.

- Valor, T., Camprodon, J., Buscarini, S., and Casals, P.: Drought-induced dieback of riparian black alder as revealed by tree 1440 rings and oxygen isotopes, For. Ecol. Manag., 478, 118500, https://doi.org/10.1016/j.foreco.2020.118500, 2020.
  - Vekuri, H., Tuovinen, J.-P., Kulmala, L., Papale, D., Kolari, P., Aurela, M., Laurila, T., Liski, J., and Lohila, A.: A widely-used eddy covariance gap-filling method creates systematic bias in carbon balance estimates, Sci. Rep., 13, 1720, https://doi.org/10.1038/s41598-023-28827-2, 2023.
- Wang, T., Zhang, H., Zhao, J., Guo, X., Xiong, T., and Wu, R.: Shifting contribution of climatic constraints on evapotranspiration in the boreal forest, Earths Future, 9, e2021EF002104, https://doi.org/10.1029/2021EF002104, 2021.
  - Warlo, H., von Wilpert, K., Lang, F., and Schack-Kirchner, H.: Black Alder (Alnus glutinosa (L.) Gaertn.) on Compacted Skid Trails: A Trade-off between Greenhouse Gas Fluxes and Soil Structure Recovery?, Forests, 10, 726, https://doi.org/10.3390/f10090726, 2019.
- Wharton, S., Schroeder, M., Paw U, K. T., Falk, M., and Bible, K.: Turbulence considerations for comparing ecosystem exchange over old-growth and clear-cut stands for limited fetch and complex canopy flow conditions, Agric. For. Meteorol., 149, 1477–1490, https://doi.org/10.1016/j.agrformet.2009.04.002, 2009.
  - Williams, C. A., Reichstein, M., Buchmann, N., Baldocchi, D., Beer, C., Schwalm, C., Wohlfahrt, G., Hasler, N., Bernhofer, C., Foken, T., Papale, D., Schymanski, S., and Schaefer, K.: Climate and vegetation controls on the surface water balance: Synthesis of evapotranspiration measured across a global network of flux towers, Water Resour. Res., 48, https://doi.org/10.1029/2011WR011586, 2012.
  - Winkler, K., Yang, H., Ganzenmüller, R., Fuchs, R., Ceccherini, G., Duveiller, G., Grassi, G., Pongratz, J., Bastos, A., Shvidenko, A., Araza, A., Herold, M., Wigneron, J.-P., and Ciais, P.: Changes in land use and management led to a decline in Eastern Europe's terrestrial carbon sink, Commun. Earth Environ., 4, 1–14, https://doi.org/10.1038/s43247-023-00893-4, 2023.
- 1460 Wolf, S., Eugster, W., Ammann, C., Häni, M., Zielis, S., Hiller, R., Stieger, J., Imer, D., Merbold, L., and Buchmann, N.: Contrasting response of grassland versus forest carbon and water fluxes to spring drought in Switzerland, Environ. Res. Lett., 8, 035007, https://doi.org/10.1088/1748-9326/8/3/035007, 2013.
- Wolf, S., Keenan, T. F., Fisher, J. B., Baldocchi, D. D., Desai, A. R., Richardson, A. D., Scott, R. L., Law, B. E., Litvak, M. E., Brunsell, N. A., Peters, W., and van der Laan-Luijkx, I. T.: Warm spring reduced carbon cycle impact of the 2012 US summer drought, Proc. Natl. Acad. Sci., 113, 5880–5885, https://doi.org/10.1073/pnas.1519620113, 2016.
  - Wutzler, T., Lucas-Moffat, A., Migliavacca, M., Knauer, J., Sickel, K., Šigut, L., Menzer, O., and Reichstein, M.: Basic and extensible post-processing of eddy covariance flux data with REddyProc, Biogeosciences, 15, 5015–5030, https://doi.org/10.5194/bg-15-5015-2018, 2018.
- Xie, J., Chen, J., Sun, G., Zha, T., Yang, B., Chu, H., Liu, J., Wan, S., Zhou, C., Ma, H., Bourque, C. P.-A., Shao, C., John, R., and Ouyang, Z.: Ten-year variability in ecosystem water use efficiency in an oak-dominated temperate forest under a warming climate, Agric. For. Meteorol., 218–219, 209–217, https://doi.org/10.1016/j.agrformet.2015.12.059, 2016.
  - Xu, H., Xiao, J., Zhang, Z., Ollinger, S. V., Hollinger, D. Y., Pan, Y., and Wan, J.: Canopy photosynthetic capacity drives contrasting age dynamics of resource use efficiencies between mature temperate evergreen and deciduous forests, Glob. Change Biol., 26, 6156–6167, https://doi.org/10.1111/gcb.15312, 2020a.
- 475 Xu, H., Zhang, Z., Xiao, J., Chen, J., Zhu, M., Cao, W., and Chen, Z.: Environmental and canopy stomatal control on ecosystem water use efficiency in a riparian poplar plantation, Agric. For. Meteorol., 287, 107953, https://doi.org/10.1016/j.agrformet.2020.107953, 2020b.
- Yang, Y., Guan, H., Batelaan, O., McVicar, T. R., Long, D., Piao, S., Liang, W., Liu, B., Jin, Z., and Simmons, C. T.: Contrasting responses of water use efficiency to drought across global terrestrial ecosystems, Sci. Rep., 6, 23284, https://doi.org/10.1038/srep23284, 2016.
  - Zhou, J., Zhang, Z., Sun, S., Yu, B., Huang, Y. G., Fang, X., Zha, T., Chen, J., Noormets, A., Guo, J., and McNulty, S.: Water-Wang, G.: The effect of vapor pressure deficit on water use efficiency of a poplar plantation in Northern China, J. For.at the subdaily time scale, Geophys. Res., 19, 483-492. Lett., 41, 5005-5013, https://doi.org/10.1007/s10310-014-0436-31002/2014GL060741, 2014.